energies

MDPI

Article

Modelling and Allocation of Hydrogen-Fuel-Cell-Based Distributed Generation to Mitigate Electric Vehicle Charging Station Impact and Reliability Analysis on Electrical Distribution Systems

Thangaraj Yuvaraj [1], Thirukoilur Dhandapani Suresh [2], Arokiasamy Ananthi Christy [3], Thanikanti Sudhakar Babu [4] and Benedetto Nastasi [5,*]

[1] Centre for Computational Modeling, Chennai Institute of Technology, Chennai 600069, India; yuvaraj4252@gmail.com
[2] Department of Electrical and Electronics Engineering, Saveetha Engineering College, Chennai 602105, India; tdsuresheee@gmail.com
[3] Department of Marine Engineering, AMET University, East Coast Road, Kanathur, Chennai 603112, India; chrisarun13@gmail.com
[4] Department of Electrical and Electronics Engineering, Chaitanya Bharathi Institute of Technology, Hyderabad 500075, India; sudhakarbabu@ieee.org
[5] Department of Planning, Design and Technology of Architecture, Sapienza University of Rome, Via Flaminia 72, 00196 Rome, Italy
* Correspondence: benedetto.nastasi@outlook.com

Abstract: The research presented in this article aims at the modelling and optimization of hydrogen-fuel-cell-based distributed generation (HFC-DG) to minimize the effect of electric vehicle charging stations (EVCSs) in a radial distribution system (RDS). The key objective of this work is to address various challenges that arise from the integration of EVCSs, including increased power demand, voltage fluctuations, and voltage stability. To accomplish this objective, the study utilizes a novel spotted hyena optimizer algorithm (SHOA) to simultaneously optimize the placement of HFC-DG units and EVCSs. The main goal is to mitigate real power loss resulting from the additional power demand of EVCSs in the IEEE 33-bus RDS. Furthermore, the research also investigates the influence of HFC-DG and EVCSs on the reliability of the power system. Reliability is crucial for all stakeholders, particularly electricity consumers. Therefore, the study thoroughly examines how the integration of HFC-DG and EVCSs influences system reliability. The optimized solutions obtained from the SHOA and other algorithms are carefully analyzed to assess their effectiveness in minimizing power loss and improving reliability indices. Comparative analysis is conducted with varying load factors to estimate the performance of the presented optimization approach. The results prove the benefits of the optimization methodology in terms of reducing power loss and improvising the reliability of the RDS. By utilizing HFC-DG and EVCSs, optimized through the SHOA and other algorithms, the research contributes to mitigating power loss caused by EVCS power demand and improving overall system reliability. Overall, this research addresses the challenges associated with integrating EVCSs into distribution systems and proposes a novel optimization approach using HFC-DG. The findings highlight the potential benefits of this approach in terms of minimizing power loss, enhancing reliability, and optimizing distribution system operations in the context of increasing EV adoption.

Keywords: electrical vehicles (EVs); spotted hyena optimizer algorithm (SHOA); bat algorithm (BA); African vulture optimization algorithm (AVOA); bald eagle search algorithm (BESA); hydrogen-fuel-cell-based distributed generation (HFC-DG); electric vehicle charging stations (EVCSs); reliability; radial distribution system (RDS)

Citation: Yuvaraj, T.; Suresh, T.D.; Ananthi Christy, A.; Babu, T.S.; Nastasi, B. Modelling and Allocation of Hydrogen-Fuel-Cell-Based Distributed Generation to Mitigate Electric Vehicle Charging Station Impact and Reliability Analysis on Electrical Distribution Systems. *Energies* **2023**, *16*, 6869. https://doi.org/10.3390/en16196869

Academic Editors: Giovanni Esposito, Yanzhou Qin, Yulin Wang and Xiao Ma

Received: 14 July 2023
Revised: 10 September 2023
Accepted: 25 September 2023
Published: 28 September 2023

1. Introduction

The rapid growth in the adoption of electrical vehicles (EVs) has presented a paradigm shift in the transport sector, driving the need for a robust and efficient charging infrastructure. Electric vehicle charging stations (EVCSs) are crucial in promoting the widespread use of EVs by offering a convenient and easily accessible way to recharge their batteries. However, the integration of these charging stations into the radial distribution system (RDS) poses unique challenges that require careful consideration and strategic planning [1,2]. On the other hand, the global evolution towards sustainable and low-carbon energy necessitates the incorporation of clean and efficient distributed generation technologies into the distribution system. Hydrogen-fuel-cell-based distributed generation (HFC-DG) emerges as a promising solution that offers numerous benefits, including reduced greenhouse gas emissions, enhanced grid stability, and increased renewable energy sources (RES) integration. HFC-DG offers numerous advantages, including high energy efficiency, environmental friendliness, scalability, fast response, fuel flexibility, low noise and vibration, and long lifespan. Because of these benefits, hydrogen fuel cells are a viable technology for decentralized power generation, with potential uses in residential, commercial, and industrial environments. This research article explores the integration of HFC-DG in the RDS and its potential to drive the transformation toward a sustainable and resilient energy infrastructure [3–5].

EVCSs can have several effects on the distribution system, including increased power demand, voltage fluctuations, power losses, and potential grid instability. However, these effects can be minimized by integrating HFC-DG into the system. Below are key effects and how they can be mitigated with the aid of HFC-DG in the RDS [6–8]:

(i) **Increased Power Demand:** EVCSs introduce additional power demand, particularly throughout maximum charging times, which can strain the distribution system. By utilizing HFC-DG units, the power required for EV charging can be supplied locally, reducing the burden on the grid and minimizing the risk of overloading distribution lines.

(ii) **Power Losses:** Increased power flows resulting from EV charging can lead to higher resistive losses in the distribution system, reducing overall system efficiency. With HFC-DG units strategically placed, power can be generated closer to the charging stations, minimizing transmission and distribution losses and improving energy efficiency.

(iii) **Voltage Fluctuations:** Rapid and simultaneous charging of multiple EVs can cause voltage deviations, leading to potential voltage instability and quality issues. The integration of HFC-DG can help regulate and stabilize voltage levels by injecting power into the system when needed, thereby mitigating voltage fluctuations and maintaining a more consistent voltage profile.

(iv) **Grid Instability:** The sudden charging demand from EVs can cause grid instability, particularly if the distribution system is not adequately prepared. By incorporating HFC-DG units, the variability in power demand from EVCSs can be mitigated. These units can provide a stable and controllable source of power, contributing to grid stability and reducing the risk of power quality issues.

Based on the above discussion, the integration of EVCSs into the distribution system leads to increased power demand, power losses, voltage fluctuations, and grid instability. However, these challenges can be mitigated through the strategic placement of HFC-DG units within the RDS. Moreover, through the localized generation of power using efficient and eco-friendly fuel cell technology, the system can alleviate the burden on the grid, stabilize voltage variations, minimize power dissipation, and bolster the comprehensive dependability and sustainability of the grid. This approach not only presents a promising avenue for skillfully managing the impact of EVCSs on the RDS but also promotes the widespread integration of EVs in an environmentally conscientious manner.

The schematic representation of the presented approach is depicted in Figure 1. HFC-DG is utilized as a solution to mitigate the impact of EVCSs on the RDS. Utilizing HFC-DG for EVCSs can alleviate the strain on the RDS, enhance grid reliability, and support the incorporation of

RESs. It offers a viable solution for minimizing the impact of EV charging on the distribution infrastructure while promoting a more sustainable and efficient energy system.

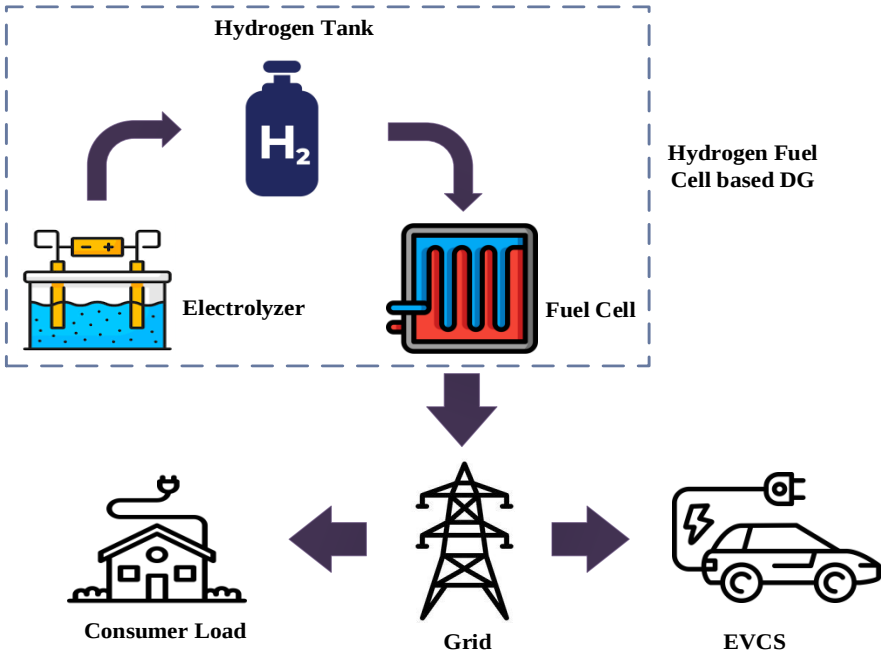

Figure 1. Schematic representation of presented approach.

2. Literature Survey

In the literature, there have been several types of research focusing on the allocation of various distribution systems, addressing various objective functions, and utilizing different optimization techniques. Research into the allocation of EVCSs is still in its initial stages and remains relatively constrained. Despite an extensive range of literature available on the placement of EVCSs in combination with Distributed Generations (DGs), flexible distribution alternating current transmission system (DFACTS) or shunt capacitors, network reconfiguration, and battery energy storage systems (BESS), both independently and simultaneously, only a few studies have addressed the real-time EVCS allocation problem. A detailed review of the allocation of EVCSs along with other energy sources is given below.

This study proposes a mathematical model for the optimum placement of EVCSs in the RDS while considering grid constraints. The primary goal is to optimize and reduce the overall expenses associated with EVCS implementation and upgrades to the RDS. The research article incorporates various factors such as load demand, grid capacity, voltage limitations, and power losses to determine the most suitable number and locations for EVCSs [9]. The study presents a stochastic optimization model that addresses uncertainties related to charging load and network security, to mitigate the overall cost of EVCS deployment and RDS reinforcement while ensuring reliable and secure system operation. To account for uncertainties, a Monte Carlo simulation approach is utilized to estimate the charging load variations [10]. Another aspect of this study focuses on optimizing the placement of EVCSs based on the vulnerability assessment of distribution networks. The vulnerability index considers factors such as power losses, voltage deviations, and reliability, and a multi-objective optimization model is suggested to identify the optimum charging station locations that minimize vulnerability while considering load demand and network constraints [11].

This study investigates the best distribution of EVCSs in the RDS while taking load variability and uncertainties into account. A two-stage stochastic programming model is developed to mitigate the total cost of ECVS and RDS reinforcement. The model accounts for the uncertainties in charging demand and generation using RESs, providing robust solutions for charging station allocation [12]. This study proposes a Transient Search Optimization (TSO)-based approach for the ideal setting of EVCSs in an RDS. The algorithm

considers factors such as load demand, power losses, voltage constraints, and transformer capacity to determine the ideal positions and sizes of EVCSs. The aim is to mitigate the overall network power losses and improve the stability of the system to satisfy the charging demand requirements [13]. The article presents a novel approach for simultaneously optimizing the sizing and situation of DGs, shunt capacitors, and EVCSs in an RDS. The use of the GOA and fuzzy multi-objective techniques adds robustness to the optimization process, enabling effective decision-making in the presence of uncertainties and conflicting objectives. The findings contribute to the development of sustainable and efficient energy systems with enhanced integration of RESs and EV infrastructure [14].

By integrating the allocation of charging infrastructure and RES, this research contributes to the development of sustainable and environmentally friendly transportation systems. It provides insights into the potential synergies between EV charging and RES generation, paving the way for more efficient and greener transportation infrastructure [15]. The article provides insights into the challenges associated with EVCSs in an RDS and proposes a coordinated charging strategy to address voltage and energy control. The research findings contribute to the development of effective strategies for managing the impact of EVCSs on an RDS, promoting the integration of EVs reliably and sustainably [16]. By considering multiple objectives, the authors provide a comprehensive analysis of the ideal allotment of fast EVCS. The results of the study demonstrate the efficiency of the presented approach in identifying a balance between cost-effectiveness, convenience, and sustainability [17].

The dynamic planning mechanism allows for the optimization of EVCS allocation over time, considering changes in demand, energy generation, and technological advancements. By dynamically adjusting the allocation strategy, the system can adapt to evolving needs and optimize the utilization of resources [18]. The study formulates the optimization problem considering various objectives. The binary bat algorithm is then applied to search for the optimal configuration of network components that satisfy these objectives [19]. The authors focus on the integration of EVs and DG into microgrids to improve energy efficiency, reliability, and sustainability. The proposed two-stage optimization approach considers the placement of EV parking lots and DG units [20]. The article presents a valuable contribution to the ideal appointment and sizing of EVCSs in a grid-tied DC microgrid. The research findings offer insights into the efficient integration of EVs and RES, contributing to the development of sustainable and resilient microgrids [21]. The results of the study demonstrate the efficiency of the planned optimization approach in achieving the appropriate allotment of EVCS and DG units in an RDS. The approach considers the temporal aspects of generation and load demand, enabling better utilization of renewable energy and improved system performance [22]. For real power loss reduction caused by EVCS, a novel integration of DSTATCOM and EVCSs is proposed in the distribution system. For the EVCS and DSTATCOM allocation challenges, two practical Indian distribution systems were investigated. Five distinct algorithms were used to demonstrate the efficacy of the provided approach [23]. The study focuses on the best placement of EVCSs using the traditional PSO algorithm. As the number of electric vehicles on the road grows, so does the importance of effective and well-planned charging infrastructure. The location of charging stations is critical in reducing costs and increasing convenience for EV owners [24]. This study proposes and compares various metaheuristic methods for evaluating the optimal placement and capacity of BESS in distribution networks with PV and EVs. The article could include case studies, simulation data, and discussions of the performance and efficacy of the algorithms used to solve the optimization problem [25].

The research article under discussion focuses on addressing the advantages of allocating HFC-DG in mitigating power loss and improving bus voltage in the context of incorporating EVCSs into an RDS. The simultaneous placement of HFC-DG and EVCSs can lead to various benefits, including power loss reduction, increased bus voltage and stability, power factor correction, and other favorable outcomes. It is worth noting that previous literature analyses have not adequately explored these advantages and have often overlooked the consideration of reliability analysis in distribution systems. The article aims to

bridge these gaps by presenting an optimal allocation strategy for HFC-DG units to minimize the impact of EVCSs in an RDS while taking into account reliability analysis. To achieve this, the authors employ a nature-inspired optimization technique called the SHOA.

Further, to demonstrate the effectiveness of the suggested technique, the authors constructed the objective function using four different algorithms: the bat algorithm (BA) [26], African vulture optimization algorithm (AVOA) [27], bald eagle search algorithm (BESA) [28], and the proposed spotted hyena optimizer algorithm (SHOA) [29]. Since there is no literature on distribution systems using EVCSs and HFC-DG for any test systems, the authors used the above algorithms to construct the same objective function and compared the results to the proposed SHOA. In addition to that, the reason behind choosing the proposed SHOA algorithm over other algorithms is given by the following:

- The SHOA excels in handling various types of constraints and delivering superior solutions compared to other powerful optimizers.
- It avoids local optima traps even with increased problem complexity and variables.
- SHOA is characterized by high convergence speed and accuracy.
- It effectively balances exploration and exploitation, ensuring a fruitful trade-off between these stages.
- Inspired by spotted hyena hunting behavior, the SHOA introduces a unique optimization approach.
- The algorithm supports parallel processing, leading to faster convergence and exploration.
- SHOA's versatility extends to both continuous and discrete optimization problems.
- With fewer tunable parameters, the optimization setup is simplified.
- As a novel optimization algorithm, the SHOA introduces fresh perspectives and strategies.
- It efficiently explores intricate solution spaces by identifying promising regions.

The objective function is designed to optimize the allocation of HFC-DG units to minimize power loss in the RDS. One significant aspect of this research article is the inclusion of reliability analysis in the evaluation of the proposed allocation strategy. Reliability analysis provides insights into the performance and robustness of the system, considering factors such as outage probability, fault conditions, and system resilience. By considering reliability analysis, the article provides a more comprehensive understanding of the proposed allocation strategy's effectiveness and its impact on system reliability.

In summary, the research article contributes to the field by focusing on the optimal allocation of HFC-DG units to minimize the effects of EVCSs in an RDS. It incorporates reliability analysis and utilizes SHOA optimization techniques to address the multi-objective nature of power loss mitigation and voltage stability enhancement. Furthermore, the study compares the performance of SHOA with the BA to assess their effectiveness in achieving the desired objectives.

The research paper presents numerous important contributions to the integration of HFC-DG in an RDS to reduce the impact of EVCS:

- **Novel Incorporation of HFC-DG:** The paper presents an innovative concept by introducing hydrogen-fuel-cell-based DG units into the RDS to address the challenges posed by EVCSs in the RDS. Unlike previous studies that used solar, wind, or diesel-based DGs, this work presents the integration of HFC-DG for EVCS mitigation.
- **Consideration of Load Levels and Battery Capacities:** While many earlier studies focused solely on constant load and single battery capacity for EVCS allocation, this research acknowledges the dynamic nature of real-world scenarios. It investigates various load levels (Light, Normal, and Peak) and three distinct battery capacities (20 kWh, 10 kWh, 16 kWh) during EVCS and HFC-DG allocation, resulting in a comprehensive assessment.
- **Application of SHOA:** This study deploys the SHOA for the EVCS and HFC-DG allocation problem, a novel approach not explored in prior research. The adoption of SHOA demonstrates its potential for optimizing the RDS configuration.

- **Inclusion of reliability analysis:** Unlike many earlier studies that overlooked reliability analysis, this research emphasizes the importance of considering reliability in the proposed methodology. By factoring in reliability, the placement of HFC-DG units is optimized to enhance the overall dependability and resilience of the distribution system.
- **Comparative analysis with multiple algorithms:** Through implementation on an IEEE 33-bus RDS, the paper evaluates four distinct optimization techniques: SHOA, BA, AVOA, and BESA. The study meticulously compares algorithm performance using various parameters, highlighting the superiority of the proposed approach and showcasing its efficacy in achieving desired outcomes.

3. Formulation of the Research Problem

3.1. Power Flow Analysis

In comparison to transmission systems, distribution systems often exhibit a higher R/X ratio. Consequently, conventional power flow analysis techniques such as Gauss–Seidel, Newton–Raphson, and quick decoupled load flow studies are insufficient for computing line flows and voltages in distribution systems. To address this challenge, this research employed the direct distribution load flow (DLF) method to assess power losses and voltage levels in each branch [30]. This paper focuses on the optimal planning of HFC-DGs and EVCSs within a distribution system. Figure 2 presents a schematic depiction of a standard distribution system, showcasing the integration of HFC-DGs and EVCS. This diagram also highlights a specific portion of the RDS, characterized by parameters such as resistance ($R_{m,m+1}$) and reactance ($X_{m,m+1}$), along with existing load and EVCS load. The distribution system comprises transmitting and receiving end buses, designated as 'm' and '$m + 1$' respectively. Correspondingly, the voltages at these buses are represented by V_m and V_{m+1}. Notably, the introduction of EVCSs at any given bus within the distribution network leads to an increase in real power consumption exclusively. The power loss can be minimized by placing the HFC-DG in the RDS. Thus, the placement of EVCS/HFC-DG becomes pivotal at the node (bus) where the branch current attains its minimum value. This strategic positioning ensures an optimal integration that contributes to system efficiency and effective power distribution.

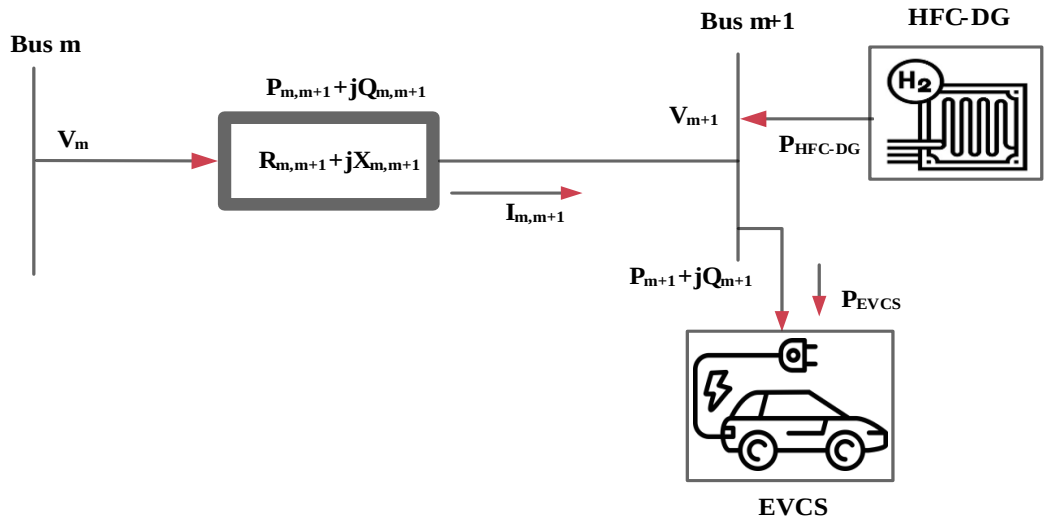

Figure 2. Single-line diagram for RDS with the presented approach.

3.1.1. Direct Load Flow Analysis

The complex load S_m of bus 'm' in distribution networks is given as

$$S_m = P_m + Q_m, \quad m = 1, 2, 3 \ldots\ldots n \tag{1}$$

where 'n' represents the total count of buses, 'P_m' signifies the active power at the 'mth' bus, and 'Q_m' represents the reactive power at the 'mth' bus. The current injection at the 'mth' bus can be formulated as follows:

$$I_m = \frac{S_m}{V_m} \tag{2}$$

Utilizing the voltage at bus 'm' denoted as V_m, a simple RDS, as depicted in Figure 2, is employed as an illustrative example to develop two relationship matrices. The establishment of these matrices involves Equation (2), allowing the transformation of power injections into their corresponding equivalent current injections. Through the application of Kirchhoff's Current Law (KCL) to the RDS configuration, a clear connection between the current injections at bus nodes and the currents flowing through branches is derived.

In this context, the branch current, designated as 'I', showcases a direct link with the bus-injection to branch-current relationship (*BIBC*). This connection can be concisely articulated as follows:

$$[I] = [BIBC][i] \tag{3}$$

Conversely, the voltage decrements (V_d) at each individual bus concerning the reference bus are computed through the utilization of Kirchhoff's Voltage Law (KVL). The interplay connecting branch currents and bus voltages can be formulated as follows:

$$[V_d] = [BCBV][I] \tag{4}$$

The branch-current to bus-voltage matrix, denoted as '*BCBV*', plays a pivotal role in the system analysis. Through Equations (3) and (4), the interrelation between bus current injections and bus voltages is elegantly conveyed:

$$[V_d] = [BCBV][BIBC][i] \tag{5}$$

$$[V_d] = [DLF][i] \tag{6}$$

The solution of the load flow problem within the RDS can be achieved by iteratively solving Equations (7)–(9).

$$I_m = \left(\frac{S_m}{V_m^i}\right)^* \tag{7}$$

$$\left[V_d^{i+1}\right] = [DLF]\left[i^i\right] \tag{8}$$

$$\left[V^{i+1}\right] = \left[V^0\right]\left[V_d^{i+1}\right] \tag{9}$$

where 'i' is the iteration count, and V^0 is the initial voltage.

3.1.2. Load Flow Calculation

The power flows are computed by the following set of simplified recursive equations derived from the single-line diagram depicted in Figure 2.

The voltage magnitude at node $m + 1$ is determined by the equation:

$$V_{m+1} = V_m - I(R_{m,m+1} + jX_{m,m+1}) \tag{10}$$

V_{m+1} indicates the voltage magnitude at bus $m + 1$ in the equation, while V_m represents the voltage magnitude at bus m. $R_{m,m+1}$ is the resistance of the line between nodes m and $m + 1$, while $X_{m,m+1}$ is the reactance of the same line.

$$i_{m+1} = \frac{(P_{m+1} + jQ_{m+1})^*}{V_m} \tag{11}$$

The current injected at node $m + 1$, denoted as i_{m+1}, is determined by the complex conjugate of the apparent power $(P_{m+1} + jQ_{m+1})$ divided by the voltage V_m at node m. In

this equation, P_{m+1} represents the real power load at bus $m + 1$, while Q_{m+1} represents the reactive power load at bus $m + 1$.

The following formula is used to calculate the system's actual and reactive power losses: The expression determines the true power loss between nodes m and $m + 1$.

$$P_{loss(m,m+1)} = \left(\frac{P_{m,m+1}^2 + Q_{m,m+1}^2}{|V_m|^2} \right) R_{m,m+1} \tag{12}$$

Similarly, the reactive power loss between nodes m and $m + 1$ is calculated using:

$$Q_{loss(m,m+1)} = \left(\frac{P_{m,m+1}^2 + Q_{m,m+1}^2}{|V_m|^2} \right) X_{m,m+1} \tag{13}$$

Here, $P_{m,m+1}$ represents the real power flow in the line connecting nodes m and $m + 1$, while $Q_{m,m+1}$ denotes the reactive power flow in the same line.

The computation of total real and reactive power losses in the system involves summing up the power losses associated with each individual branch. Equation (14) represents this calculation, with nb denoting the total count of branches within the system.

$$P_{T,Loss} = \sum_{m=1}^{nb} P_{Loss}(m, m + 1) \tag{14}$$

3.2. DG Using Hydrogen Fuel Cell Technology

Hydrogen fuel cell technology can be effectively utilized for distributed generation applications. While hydrogen-fuel-cell-based DG offers numerous advantages, challenges such as hydrogen storage and infrastructure, cost considerations, and technology maturity need to be addressed for widespread adoption. Nonetheless, hydrogen fuel cell technology holds significant potential for clean, efficient, and sustainable distributed generation applications. HFC-DG is gaining increasing attention as a result of its notable efficiency and distinctive environmentally friendly characteristics [31].

In recent years, fuel cell technology has gained significant prominence as a form of distributed generation resource. The proton-exchange membrane fuel cell (PEMFC) has gained popularity as the preferred choice for distributed generation applications, owing to its numerous benefits. These advantages encompass exceptional effectiveness and power compactness, extended lifespan, minimal wear and tear, and efficient operation within a temperature range of 40–80 degrees Celsius. Notably, this temperature range enables the PEMFC to have a fast start-up speed, adding to its overall appeal and practicality as a distributed generation solution.

Figure 3 depicts the relationship between voltage and current, known as the polarization curve, in a fuel cell stack. When the current within the fuel cell rises, there is a corresponding decrease in voltage at both terminals. The current–voltage relationship in a PEMFC reveals three distinct operational zones. The initial operational zone is known as the ohmic region, where the fuel cell's voltage experiences a linear decline with increasing current. This region represents the practical operating range of the fuel cell, ensuring efficient and dependable performance. The second operational zone is referred to as the concentration region. In this region, the current exceeds the upper limit, causing a significant drop in the fuel cell voltage. Operating the fuel cell in this condition for an extended period should be avoided as it can lead to severe damage to the equipment due to hydrogen depletion. Therefore, it is crucial to function the fuel cell within its practical operational range (ohmic region) to ensure reliable and safe long-term operation. Operating the fuel cell beyond the upper limit (concentration region) can have detrimental effects and should be avoided to maintain the performance and integrity of the equipment [32].

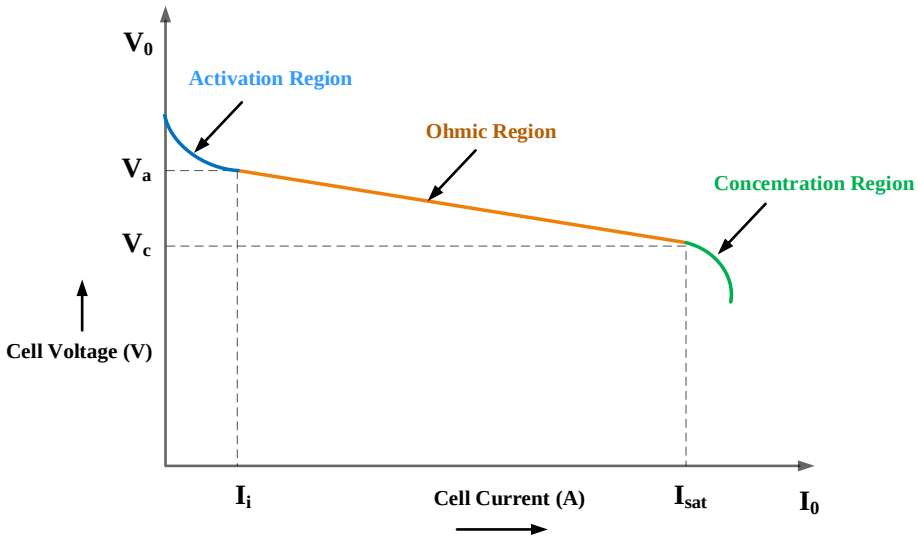

Figure 3. V-I characteristics of fuel cell.

The following equations represent the current–voltage characteristics of a PEMFC.

$$V_{HFC} = V_{cp} - V_a - V_p - V_c \tag{15}$$

$$V_a = n_{cell} * log\left(\frac{i_{HFC} - i_i}{i_o}\right) \tag{16}$$

$$V_p = r * (i_{HFC} - i_i) \tag{17}$$

$$V_c = \alpha * log\left(1 - \left(\frac{i_{HFC} - i_i}{i_{lt}}\right)\right) \tag{18}$$

$$V_{cp} = \tau_1 + \tau_2(t - 298.15) + \tau_3 t[ln(p_{H2}) + 0.5ln(p_{O2})] \tag{19}$$

$$P_{HFC-DG} = m_{cell} * \left\{V_{TD} - \left[\alpha * log\left(\frac{I_{HFC}}{n_{cell}}\right)\right] - \left[r * \left(\frac{I_{HFC}}{n_{cell}}\right)\right] - \left[SP * e^{\left(\frac{n * I_{HFC}}{n_{cell}}\right)}\right]\right\} * I_{HFC} \tag{20}$$

The power output of a PEMFC, labeled as P_{HFC-DG}, is measured in Watts. The reversible voltage of the fuel cell, denoted as V_{TD}, is determined by its thermodynamic potential difference. V_{HFC} represents the voltage across the fuel cell, while V_{cp} signifies the voltage generated by chemical reactions. It accounts for the voltage drop caused by the chemical reaction occurring at both the anode and cathode. V_p represents the voltage drop resulting from proton permeation through the solid electrolyte and electron passage through the intrinsic resistance. Lastly, V_c corresponds to the voltage drop caused by gas transmission resulting from chemical reactions. The current supplied by the fuel cell is referred to as i_{HFC}, whereas i_i represents the internal current. i_0 denotes the exchanged current, and i_{lt} indicates the current that is limited. The resistance of the membrane and connectors is symbolized by r, and α represents the coefficient of mass transmission. Furthermore, the symbol SP represents the standard potential of the chemical reaction between O_2 and H_2 in volts. I_{HFC} represents the electric current output of the fuel cell, measured in amperes. The parameter m_{cell} signifies the number of cells connected in series within the fuel cell system, while n_{cell} represents the surface area of each individual cell, measured in square centimeters. The coefficient τ is used to indicate the specific type of fuel cell being employed, and t represents the operating temperature of the system. The values p_{H2} and p_{O2} correspond to the input pressures of hydrogen and oxygen, respectively.

Modelling of Hydrogen-Fuel-Cell-Based DG for RDS

Strategically situating HFC-DG units within the RDS offers a multitude of advantages. These encompass decreased line losses, enhanced bus voltage, regulation of power factor, among other benefits. The ensuing equations serve as guiding principles for the seamless integration of HFC-DG into the distribution infrastructure.

Upon the introduction of real power via HFC-DG at terminal m, the resultant net real power (P_T) can be described as follows.

$$P_T = P_{m+1} - P_{HFC-DG} \tag{21}$$

In Figure 2, the real power loss after placing the HFC-DG at bus m is given as:

$$P_{loss(m,m+1)} = \left(\frac{P_T^2 + Q_T^2}{|V_t|^2}\right) R_{m,m+1} \tag{22}$$

$$P_{loss(m,m+1)} = \left(\frac{(P_{m+1} - P_{HFC-DG})^2 + (Q_{m+1})^2}{|V_m|^2}\right) R_{m,m+1} \tag{23}$$

$$P_{loss(m,m+1)} = \left(\frac{P_{m,m+1}^2 + Q_{m,m+1}^2}{|V_m|^2}\right) R_{m,m+1} + \left(\frac{P_{HFC-DG}^2 - 2P_{m+1} * P_{HFC-DG}}{|V_m|^2}\right) R_{m,m+1} \tag{24}$$

The reduction in power loss, represented as $\Delta P_{T,Loss}^{HFC-DG}$, signifies the variation in system losses before and after the installation of an HFC-DG in the RDS. These quantities can be formulated as follows:

$$\Delta P_{T,Loss}^{HFC-DG} = \left(\frac{P_{DHFC-DG}^2 - 2P_{m+1} * P_{HFC-DG}}{|V_m|^2}\right) R_{m,m+1} \tag{25}$$

To some extent, the introduction of HFC-DG units has a good impact on lowering distribution network losses.

3.3. Modelling of EVCS Load for RDS

EVCSs impose an additional burden on the RDS, increasing its overall load. Equation (26) can be utilized to assess the total load on the distribution system following the integration of EVCSs.

$$P_{Load} = \sum_{m=1}^{nb} \left(P_{avilable,m+1} + P_{EVCS(m+1)}\right) \tag{26}$$

In the given equation, P_{Load} denotes the total load, $P_{avilable,m+1}$ denotes the load already present on the $m + 1$ bus, and $P_{EVCS(m+1)}$ represents the load from an EVCS connected to the $m + 1$ bus. The necessary information for calculating the necessary energy for battery charging using Equations (27) and (28) is derived from the reference [33]. The modelling of the EVCS follows:

$$P_{EVCS} = n_{EV} * B_c * S_c \tag{27}$$

$$S_c = n_T - SOC_{PS} \tag{28}$$

The expression P_{EVCS} represents the overall power requirement from an *EVCS*. B_c denotes the kWh rating of the battery, while S_c represents the amount of charging needed in terms of *SOC*. SOC_{PS} indicates the present state of the *SOC*, and n_{EV} & n_T stand for the number and total of EVs respectively.

3.4. Indices of Distribution Network Reliability

The field of research focused on reliability in electrical distribution systems has gained significant importance over time. Reliability, in this context, refers to the probability of a system operating satisfactorily within defined operating constraints for a given duration. Within the realm of electrical network reliability studies, the primary objective is to ensure

the dependable functioning of generation, transmission, and distribution processes. The satisfaction level of consumers is closely linked to the reliability of the RDS. To evaluate the dependability of an RDS, it is necessary to gather quantitative data regarding failure rates, repair rates, average outage duration, and the number of affected consumers at different load points. These metrics play a crucial role in determining reliability indices, which provide a quantitative assessment of various aspects of system performance [2]. To ensure accurate and reliable evaluations of system reliability, it is important to carefully select the appropriate set of indices based on the specific application.

3.4.1. Computation of Statistical Metrics for Reliability at Various Load Conditions

Failure rate, repair rate, and average outage time are statistical characteristics that have a substantial impact on dependability indices. These parameters can be computed for various load points, particularly the jth load point.

$$\text{Average failure rate } (\alpha_j) = \sum_{i \epsilon l} (n_i * f_i) \ \ (\text{failure/yr}) \tag{29}$$

$$\text{Annual repair rate } (\beta_j) = \sum_{i=l} (n_i * \Delta_{ji}) \ \ (\text{hr/yr}) \tag{30}$$

$$\text{Average outage duration } (\gamma_j) = \frac{\alpha_j}{\beta_j} \ (\text{hr}) \tag{31}$$

The failure rate of the ith element in the distribution system is denoted as f_i, where l represents a specific element in the system consisting of a total of l elements. The quantity of elements of type ith in the distribution system is represented by n_i. The time of failure at the jth load point resulting from the failure of the ith element is indicated by Δ_{ji}. The average failure rate at the jth load point is denoted as α_j, and the annual outage duration at the jth load point is represented by β_j.

3.4.2. Formulas for Reliability Indicators in Distribution Systems

The classification of reliability indices in an RDS can be separated into two categories: load-oriented and customer-oriented indices, as depicted in Figure 4. When conducting reliability analysis in an RDS, a variety of indices, including both load-oriented and customer-oriented measures, are utilized. These indices are accompanied by mathematical formulas, as mentioned in reference [34].

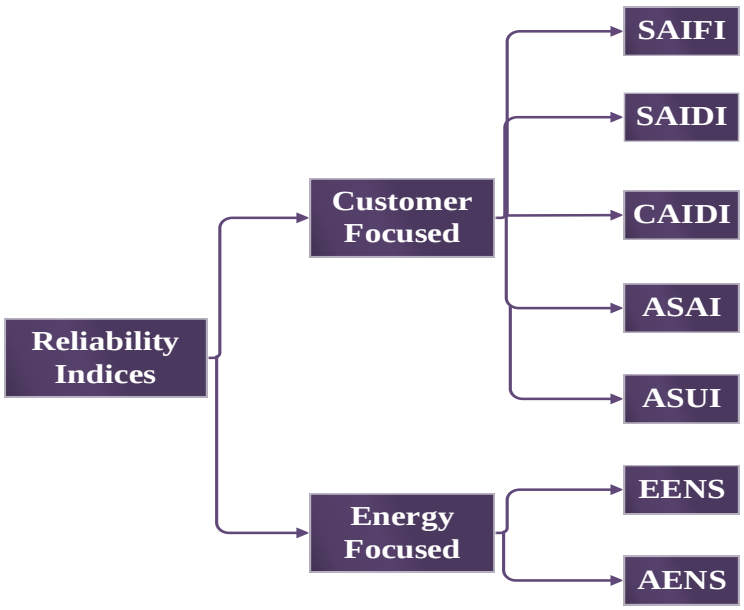

Figure 4. Various reliability indices in RDS.

(i) **Customer-focused dependability indices** The utilization of these indices has enhanced the reliability of power systems by focusing on improving consumer satisfaction and load service quality. Here is an elaborate outline and mathematical formulation of various reliability indices that prioritize customer needs.

(a) **System Average Interruption Frequency Index (SAIFI):** It is a statistic used to analyze a system's condition in terms of interruptions. It is computed by dividing the total number of outages in a year by the total number of customers served during that time period. SAIFI quantifies the frequency of failures in terms of interruptions per customer per year, as represented by Equation (32) in the context of the study.

$$SAIFI = \frac{\sum_j^{l_j} \alpha_j N_j}{\sum_j^{l_j} N_j} \text{ (failures/customer/yr)} \tag{32}$$

(b) **System Average Interruption Duration Index (SAIDI):** SAIDI is a reliability metric used to assess the condition of an electrical system in relation to its downtime. The calculation involves dividing the cumulative number of uninterrupted service disruptions by the annual number of customers (33) served. SAIDI is typically expressed as the number of hours of downtime experienced by each customer over the course of a year.

$$SAIDI = \frac{\sum_j^{l_j} \beta_j N_j}{\sum_j^{l_j} N_j} \text{ (hr/customer/yr)} \tag{33}$$

(c) **Customer Average Interruption Duration Index (CAIDI):** The described metric is a measure of reliability that quantifies the proportion of time customers experience uninterrupted service within a given year relative to the total number of service interruptions. This metric, denoted as Hr/customer/interruption, calculates the average duration of outages per customer and is determined using Equation (35).

$$CAIDI = \frac{SAIDI}{SAIFI} \tag{34}$$

$$CAIDI = \frac{\sum_j^{l_j} \beta_j N_j}{\sum_j^{l_j} \alpha_j N_j} \text{ (hr/customer/iterruption)} \tag{35}$$

(d) **Average Service Availability Index (ASAI):** The concept is denoted by the term "per unit" (p.u.), indicating the ratio between the total number of hours available in a year and the desired hours, as expressed in Equation (36).

$$ASAI = \frac{\sum(N_j * 8760) - \sum_j^{l_j} \beta_j N_j}{\sum(N_j * 8760)} \text{ (p.u.)} \tag{36}$$

(e) **Average Service Unavailability Index (ASUI):** The measurement is denoted per unit (p.u.) and is calculated by dividing the total annual duration of service unavailability by the desired total hours, as specified in Equation (37).

$$ASUI = 1 - ASAI \text{ (p.u.)} \tag{37}$$

(ii) **Energy-focused dependability indices** The determination of energy-oriented reliability indices takes place at various load points.

(a) **Expected Energy Not Supplied (EENS):** The energy insufficiency, given in MWh/yr, is quantified as the sum of all consumers' EENS according to Equation (38). *EENS* serves as an indicator of insufficient energy supply.

$$EENS_j = A_j \beta_j \ (\text{MWh/yr}) \tag{38}$$

(b) **Average Energy Not Supplied (AENS):** This index quantifies the amount of unserved energy over a specific time period, as represented by Equation (39). It is measured in MWh/customer/yr.

$$AENS = \frac{\sum_j^{l_j} A_j \beta_j}{\sum_j^{l_j} N_j} \ (\text{MWh/customer/yr}) \tag{39}$$

Each load point is characterized by its average demand, denoted as A_j, and the expected *ENS*, represented as $EENS_j$. The variable l_j represents the total count of load points, while N_j corresponds to the overall number of consumers at the *j*th load point. The process of calculating reliability indices involves multiple steps, as depicted in Figure 4.

Power system network interruptions can occur due to various causes, including the following:

- Disturbances resulting from outages;
- Interruptions caused by equipment failures within the power system;
- Load shedding as a response to sudden increases in demand;
- Planned interruptions for equipment maintenance and preservation.

3.5. Objective Function

The primary impartiality of this research is to identify the most effective locations for EVCSs and HFC-DG within the RDS. When integrating EVCSs into the power grid, there is a rise in power loss and a decrease in the quality of the bus voltage. To address these challenges, HFC-DGs are strategically positioned at optimal nodes in the distribution system. This allocation process ensures that the voltage levels at each point in the system remain within acceptable limits. The primary aim of the objective function is to minimize power loss in the distribution system, while also considering the imposed constraints. By doing so, it enhances the reliability of the system, maximizes voltage stability, and improves the overall voltage profile. The mathematical expression of the objective function is presented below.

$$Minmize(F) = Min(P_{T,Loss}) \tag{40}$$

where $P_{T,Loss}$ is the total power loss of the RDS.

3.6. System Constraints

The optimization process for the RDS concerning the allocation of HFC-DG and EVCSs is executed by leveraging the SHOA. This optimization procedure ensures that the allocation of HFC-DG and EVCS units adheres to the defined equality and inequality constraints without any violations. These constraints play a critical role in maintaining the stability, efficiency, and feasibility of the optimized distribution system.

3.6.1. Equilibrium of Power

The subsequent statement presents power balance constraints formulated as equality constraints.

$$P_{TLoss} + \sum P_{D(m)} + \sum P_{EVCS(m)} = \sum P_{HFC-DG(m)} \tag{41}$$

The expression $P_{D(m)}$ denotes the power required at two specific bus locations denoted by *m*. Similarly, $P_{HFC(m)}$ represents the power produced by utilizing HFC-DG, and $P_{EVCS(m)}$ signifies the power consumption attributed to EVCS.

3.6.2. Voltage Magnitude

$$V_{m,min} \leq |V_m| \leq V_{m,max} \tag{42}$$

The minimum voltage limits of the buses are denoted as $V_{m,\min}$, while the maximum voltage limits are represented by $V_{m,\max}$.

3.6.3. Power Compensation

The actual limitations on power can be defined as the amount of injected power at designated bus locations, which must remain within their authorized boundaries.

$$P^{min}_{HFC-DG(m)} \leq P_{EHFC-DG(m)} \leq P^{max}_{HFC-DG(m)} \quad \text{t} = 1, 2, \ldots\ldots\ldots nb \tag{43}$$

The symbol $P^{\min}_{HFC-DG(m)}$ refers to the lower bound of the real power limits for compensated bus m, while $P^{\max}_{HFC-DG(m)}$ represents the upper bound of the real power limits for compensated bus m.

4. Proposed Optimization Approach

This section outlines the conceptual framework of the SHOA and its application in solving the HFC-DG and EVCS allocation problem in the RDS.

4.1. SHOA Overview

The behavior of the spotted hyena exhibits intriguing parallels with certain aspects of human social behavior. Notably, they exhibit unwavering determination in scavenging for sustenance and survival, often residing in organized groups. At a certain stage of development, male hyenas depart from their birth group and integrate into a different clan for a significant duration. Intriguingly, these creatures employ various sensory mechanisms to identify familiar individuals, and they communicate vital information such as the discovery of new food sources through alert vocalizations. The SHOA, employed in this study, draws inspiration from the hunting and social behaviors of these remarkable animals. By emulating these principles, the SHOA adeptly navigates diverse types of constraints, yielding superior solutions compared to other robust optimization techniques. Moreover, it effectively sidesteps the pitfall of becoming trapped in local optima, even when dealing with intricate optimization challenges characterized by a high volume of problem variables. The method's exceptional convergence speed and accuracy further underscore its efficacy [29].

The SHOA is an optimization technique that follows a series of steps and equations to search for the best solution for a given problem.

(i) **Encircling prey:** The optimization process considers different search factors and consistently adjusts the best position relative to the target for achieving the optimal solution. The exact mathematical equation for expressing this behavior may vary based on the specific problem under consideration.

$$R_{hp} = \left| Y * v_p(t) - v_h(t) \right| \tag{44}$$

$$v_h(t+1) = v_p(t) - Z * R_{hp} \tag{45}$$

In the given context, R_{hp} represents the separation between a spotted hyena and its prey, while v_p denotes the position vector of the prey. Similarly, v_h represents the position vector of the spotted hyena. The variable t indicates the current iteration, and Y and Z symbolize vectors containing coefficient factors.

$$Y = 2v_{r1} \tag{46}$$

$$Z = 2l * v_{r2} - l \tag{47}$$

$$l = 5 - \left(Iter * \left(\frac{5}{Max_{Iter}} \right) \right) \tag{48}$$

Here, $Iter = 0, 1, 2, \ldots\ldots\ldots\ldots\ldots\ldots Max_{Iter}$

The random vectors v_{r1} and v_{r2} are within the range of [0, 1], and the value of l can be linearly decreased from 5 to 0.

(ii) **Hunting:** The hunting strategy of the SHOA is explained as follows.

$$R_{hp} = \left| Y * v_{p,best}(t) - v_{h,best}(t) \right| \tag{49}$$

$$v_{h,best} = v_{p,best} - Z * R_{hp} \tag{50}$$

$$Op_h = v_{h,best} + v_{h,best+1} + \cdots\ldots\ldots\ldots v_{h,best+N_h} \tag{51}$$

The spotted hyena's optimal location relative to the prey is designated as $v_{p,best}$, while another position is denoted as $v_{h,best}$. The total count of spotted hyenas, represented as N_h, is determined by the following equation.

$$N_h = C_n \left(v_{p,best}, v_{p,best+1}, v_{p,best+2}, \ldots\ldots\ldots\ldots \left(v_{p,best+G} \right) \right) \tag{52}$$

In order to calculate N_h, a random vector G is generated, which falls between the values of 0.5 and 1. The variable n denotes the total number of answers, encompassing both the reference answers and the counted ones. C_n represents a collection of optimal answers with a size of N_h.

(iii) **Attacking prey (exploitation):** The mathematical formula for the predator's attack strategy can be expressed as follows:

$$v_h(x+1) = C_n / N_h \tag{53}$$

The velocity vector, $v_h(x+1)$, captures the optimal direction for pursuit and updates the positions of other variables in relation to the optimal position found in the search process.

(iv) **Search for prey (exploration):** Equation (47) requires the value of Z to be either greater than 1 or less than 1 for accurate determination. Another vital element of SHOA is vector Y, comprising random values. These random values assign arbitrary weights to the prey using Equation (46). If vector Y holds values greater than 1, they take precedence over values less than 1. This prioritization amplifies SHOA's exploration prowess, infusing additional randomness, and accounting for distance effects.

4.2. SHOA Implemetaion

Below are the steps outlining the implementation of the SHOA for solving the HFC-DG and EVCS allocation problem. Also, Figure 5 depicts the flowchart illustration of SHOA for the EVCS allocation with HFC-DG.

Step 1 (Set Optimization Parameters): Define the necessary parameters for the optimization process, such as:

- PopSize: Population size;
- MaxIter: Maximum number of iterations;
- Repetition: Number of repetitions;
- NumVariables: Number of variables (location and size of HFC-DG and EVCS);
- Variables' constraints.

Step 2 (Generate Initial Population): Generate the initial population matrix Population, where each row represents a member of the population, and each column corresponds to the bus number for installing HFC-DG and EVCS. Priority is given to buses with higher loss sensitivity.

Step 3 (Calculate Objective Function): Calculate the objective function for each member in the population, considering constraints. Identify the hyena (solution) with the lowest cost as the representative $\text{Hyena}_{\text{Best}}$.

Step 4 (Update SHOA Population): Apply the SHOA algorithm to update the population for the next iteration. Equations (44)–(51) are employed to facilitate the Encircling Prey and Hunting strategy specifically within the context of the HFC-DG and EVCS allocation problem.

Step 5 (Discretization and Objective Function Update): Round variables of each member to the nearest integer to move to discrete search space. Recalculate the objective function considering constraints for all members. If the new member's objective function is better than the one obtained in Step 3, replace it.

Step 6 (Termination Criterion): Check if the number of iterations exceeds the maximum iterations number (Max_{Iter}). If not, return to Step 4. Otherwise, terminate the SHOA process.

After the termination criterion is met, extract and present the optimization results:

Locations and Sizes: The optimized locations and sizes of HFC-DG and EVCS installations obtained from $\text{Hyena}_{\text{Best}}$.

Network Performance Metrics: Calculate power loss and minimum network voltage at each load level for the optimized solution.

These results provide valuable insights into the optimal allocation of HFC-DG and EVCSs in the distribution system and their impact on network performance.

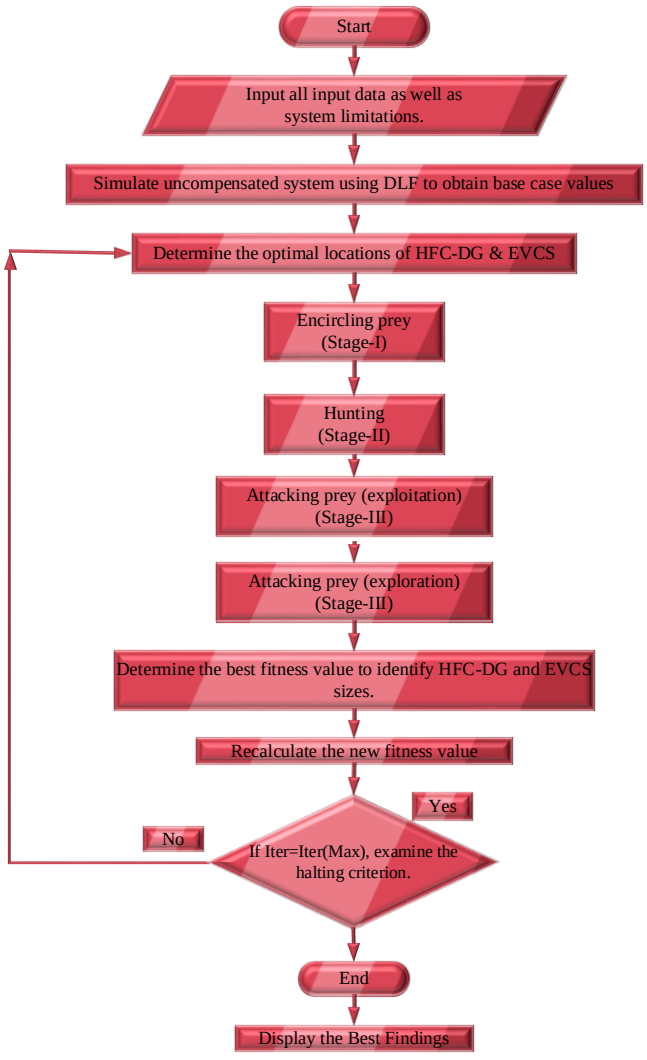

Figure 5. The execution illustration of SHOA.

5. Discussion and Findings

The proposed SHOA technique is implemented on a typical IEEE 33-bus RDS to optimize the placement and capacity of HFC-DG and EVCSs to assess its effectiveness. MATLAB is used to create the power flow algorithm for the RDS's base case real and reactive power losses and bus voltage values. The objective function is formulated using the proposed SHOA and other algorithms to showcase the applicability of the suggested technique. Due to the absence of pre-existing radial distribution systems that met the specified conditions in the available literature, the authors constructed an identical objective function using the BA algorithm. They subsequently compared the outcomes obtained through the BA algorithm with the suggested SHOA approach. Utilizing both the SHOA and BA algorithms, the authors were able to determine suitable locations and sizes for HFC-DG and EVCS.

This study explores the integration of three different types of EVs at EVCSs. These EVs have varying battery energy capacities, specifically 20 kWh, 10 kWh, and 16 kWh. Additionally, the EVs at the charging station are expected to have different states of charge (SOC). The charging station is expected to have 100 EVs, resulting in an additional power demand of 966 kW on the system. An RDS is designed to support up to two EVCSs with multiple charging ports, as well as up to two HFC-DGs. The study examines five possible cases for the integration of EVCSs and HFC-DGs within the IEEE 33-bus RDS.

5.1. IEEE 33-Bus System

The provided information describes Figure 6, which represents a single-line diagram of an IEEE 33-bus RDS equipped with two HFC-DGs and EVCSs. EVCSs are assumed to have 100 charging points, and each charger consumes 966 kW. So, EVCSs can charge 100 EVs at the same time. The optimal number of EVCSs needs to be placed at the optimal bus in the distribution network. Since EVCS installation increases the active power loss of the network, hence HFC-DGs are optimally placed to compensate for the losses due to installed EVCS. In the proposed method, two EVCSs are optimally located at the 2nd and 19th buses in the RDS. To reduce the impact of EVCSs in the RDS, two HFC-DGs are placed optimally at the 6th and 14th buses using the proposed SHOA algorithm. HFC-DG has a significant impact on mitigating the challenges posed by EVCSs within the RDS. By providing load-balancing capabilities, these fuel cells offer supplementary power during peak demand periods, effectively alleviating stress on the grid and minimizing power losses and voltage deviations. Moreover, their ability to regulate voltage levels ensures consistent power quality, addressing potential disruptions caused by simultaneous EV charging. These fuel cells also contribute to grid resilience by furnishing backup power during outages, ensuring uninterrupted charging services. Furthermore, their localized generation reduces transmission congestion and associated losses, enhancing the overall efficiency of the distribution network. With the added advantage of environmental sustainability due to their emissions-free operation, fuel-cell-system-based DGs offer an optimal solution for reducing the adverse effects of EVCSs on RDSs.

The load and line data for this system are sourced from reference [35]. The system has a real power demand of 3.72 MW and reactive power demand of 2.3 MVAr. The DLF method is employed to determine the base bus voltages and power flow across the system's lines. To achieve higher objective values, a minimum of two compensators, depending on the case, are strategically inserted at different locations in the RDS using various algorithms. The performance of the IEEE 33-bus system under various load factors and the considered cases is presented in Table 1. The table provides information on power loss, minimum voltage, and stability, as well as the size and locations of HFC-DG and EVCSs using the presented SHOA approach for all three practical load levels.

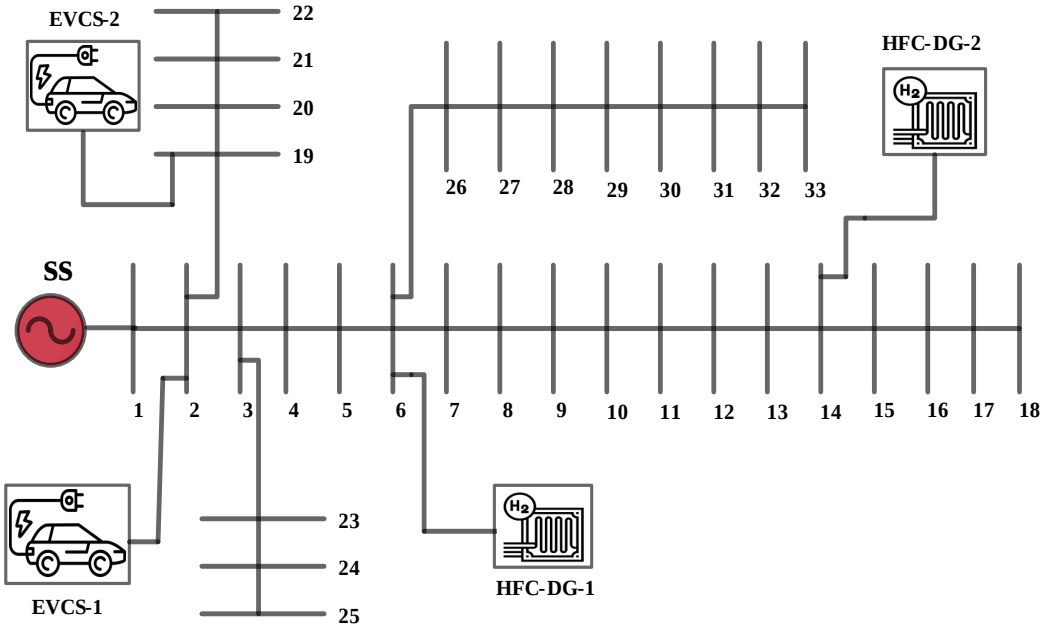

Figure 6. IEEE 33-bus test system with the proposed approach.

Table 1. IEEE 33-bus system performance under various load factors using the proposed SHOA.

Cases	Parameter	Load Factors		
		Light (0.5)	Normal (1.0)	Peak (1.6)
Case I (Without Compensation)	P_{loss} (kW)	47.07	202.67	575.34
	Q_{loss} (kVAr)	31.37	135.24	384.53
	V_{min} (p.u.)	0.9583	0.9131	0.8527
	VSI_{min} (p.u.)	0.8402	0.6890	0.5192
Case II (With One EVCS)	Optimum size (kW) and position of EVCS	966 (2)	966 (2)	966 (2)
	P_{loss} (kW)	49.78	207.84	584.01
	Q_{loss} (kVAr)	32.79	137.95	389.15
	V_{min} (p.u.)	0.9577	0.9124	0.8521
	VSI_{min} (p.u.)	0.8381	0.6871	0.5175
Case III (With Two EVCSs)	Optimum size (kW) and position of EVCS	966 (2) 966 (19)	966 (2) 966 (19)	966 (2) 966 (19)
	P_{loss} (kW)	54.92	215.82	595.96
	Q_{loss} (kVAr)	36.03	142.86	396.39
	V_{min} (p.u.)	0.9571	0.9118	0.8514
	VSI_{min} (p.u.)	0.8361	0.6853	0.5159
Case IV (With Two EVCSs and One HFC-DG)	Optimum size (kW) and position of EVCS	966 (2) 966 (19)	966 (2) 966 (19)	966 (2) 966 (19)
	Optimum size (kW) and position of HFC-DG	1250 (6)	2500 (6)	4000 (6)
	P_{loss} (kW)	29.93	111.08	290.99
	% P_{loss} Reduction	45.5	48.53	51.17
	Q_{loss} (kVAr)	21.12	79.21	208.07
	V_{min} (p.u.)	0.9746	0.9487	0.9151
	VSI_{min} (p.u.)	0.8993	0.8041	0.6915
Case V (With Two EVCSs and Two HFC-DGs)	Optimum size (kW) and position of EVCS	966 (2) 966 (19)	966 (2) 966 (19)	966 (2) 966 (19)
	Optimum size (kW) and position of HFC-DG	945 (6) 300 (14)	1900 (6) 600 (14)	3200 (6) 970 (14)
	P_{loss} (kW)	26.59	96.67	249.32
	% P_{loss} Reduction	51.58	55.21	58.16
	Q_{loss} (kVAr)	18.32	67.23	174.24
	V_{min} (p.u.)	0.9762	0.9521	0.9232
	VSI_{min} (p.u.)	0.9040	0.8136	0.7133

The proposed SHOA yields outstanding performance across various load factors. Under load factor scenarios of 0.5, 1.0, and 1.6, both Case IV (45.5%, 48.53%, and 51.17%) and Case V (51.58%, 55.21%, and 58.16%) exhibit consistently uniform power loss reduction percentages. This uniformity underscores SHOA's robustness in optimizing system efficiency regardless of load variations. Notably, SHOA excels in enhancing voltage stability and magnitude network-wide, maintaining favorable voltage parameters despite load fluctuations.

This resilience ensures dependable power delivery even amidst EVCS challenges in the RDS. By synergizing SHOA's capabilities, this approach effectively counters the potential negative impacts of EVCSs on the distribution network. Seamlessly integrating SHOA optimizes power loss reduction and ensures voltage stability and magnitude management. This approach holds great promise in fortifying the RDS against EVCS-induced perturbations, enhancing overall resilience and efficiency. Notably, Case V surpasses Case IV in loss reduction, stability, and bus voltage enhancement, further emphasizing its capacity to enhance distribution system performance.

5.2. Effect of HFC-DG and EVCS Allocation on RDS

The optimal integration of HFC-DG and EVCSs requires careful consideration of technical, operational, and planning aspects to mitigate power loss, bus voltage, and reliability issues in the RDS created by EVCS. The following sections explain the effect of HFC-DG and EVCS allocation on the RDS.

5.2.1. Effect of EVCSs on System Power Loss

The initial analysis indicates that in the 33-bus RDS, the base case experiences an active power loss of 202.67 kW and a reactive power loss of 135.24 kVAr. When one EVCS is introduced at the 2nd bus, the power loss in the RDS increases to 207.84 kW. Installing two EVCSs optimally at the 2nd and 19th bus locations further raises the power loss to 215.82 kW. In order to promote the widespread adoption of EVs, it is recommended to install a larger number of EVCSs along routes frequently used by EV users. However, it is important to consider that while the addition of EVCSs is crucial for the success of EVs, it can have negative effects on the health of the power distribution system. Therefore, a balance must be struck between the well-being of the power system and the establishment of charging arrangements. To mitigate the effect of EV charging on the RDS, HFC-DGs are incorporated. By strategically placing a 2500 kW HFC-DG at bus number 6, a significant reduction of 111.08 kW in real power loss is achieved. Additionally, placing two HFC-DGs at buses 6 and 14, with capacities of 1900 kW and 600 kW, respectively, results in a reduced loss of 96.67 kW.

The presented approach delves into real-time scenarios by examining the system across three distinct load levels. The impact of EVCSs on both real and reactive power losses has been comprehensively analyzed through the application of the SHOA. The findings are systematically organized in Table 2, offering insights into the influence of EVCSs on various load levels. Figure 7 serves as a visual representation of the effect of EVCSs on real and reactive power losses specifically under light load conditions (0.5). This analysis is conducted with a focus on 50% of the total real power load (1.86 MW) from the overall load of 3.72 MW. To provide context, Case IV and Case V are juxtaposed against Case III, which serves as the baseline for comparison in both cases IV and V. Crucially, the application of SHOA-based optimization emerges as a key factor in mitigating real and reactive power losses. By enhancing the performance of both Case IV and Case V, the SHOA approach effectively outperforms the base Case III. This signifies the algorithm's proficiency in addressing power loss concerns, both in terms of real and reactive power components, under varying load conditions.

Table 2. Effect on real and reactive power losses due to EVCSs on various load factors.

Cases	Load Factors					
	0.5		1.0		1.6	
	P_{loss} (kW)	Q_{loss} (kVAr)	P_{loss} (kW)	Q_{loss} (kVAr)	P_{loss} (kW)	Q_{loss} (kVAr)
Case I	47.07	31.37	202.67	135.24	575.34	384.53
Case II	49.78	32.79	207.84	137.95	584.01	389.15
Case III	54.92	36.03	215.82	142.86	595.96	396.39
Case IV	29.93	21.12	111.08	79.21	290.99	208.07
Case V	26.59	18.32	96.67	67.23	249.32	174.24

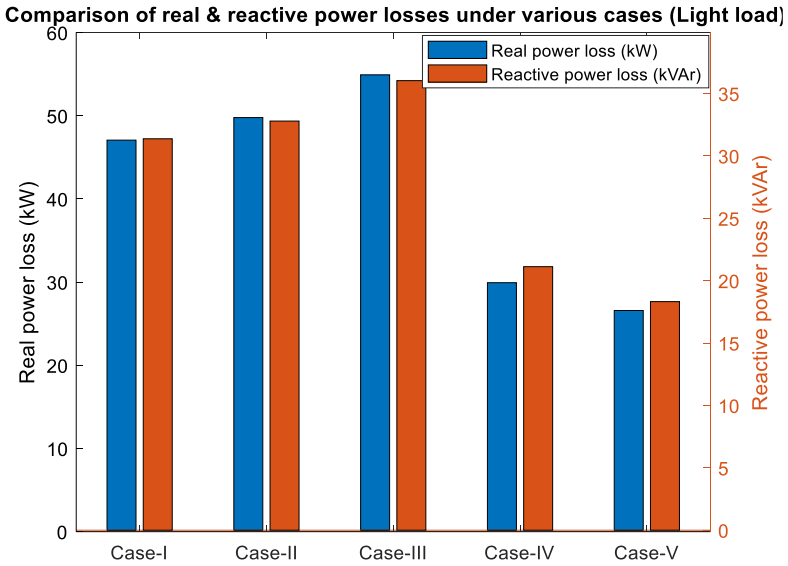

Figure 7. Effect of EVCSs on real and reactive power losses on light load (0.5).

Figure 8 provides a visual representation of the impact of EVCSs on real and reactive power losses under normal load conditions (1.0). For the purposes of this study, the entire real power load (100%) has been taken into consideration. It is worth noting that this specific scenario holds significant importance, as it has been widely adopted by researchers when addressing the EVCS allocation problem. In this context, the real and reactive power loss profiles of Case IV and Case V are directly compared with the baseline Case III. The application of the SHOA brings about a noteworthy outcome: a substantial reduction in power losses resulting from EVCS integration. Specifically, SHOA-based optimization achieves a 50% reduction in power losses compared to the base case, attributed to the presence of EVCS.

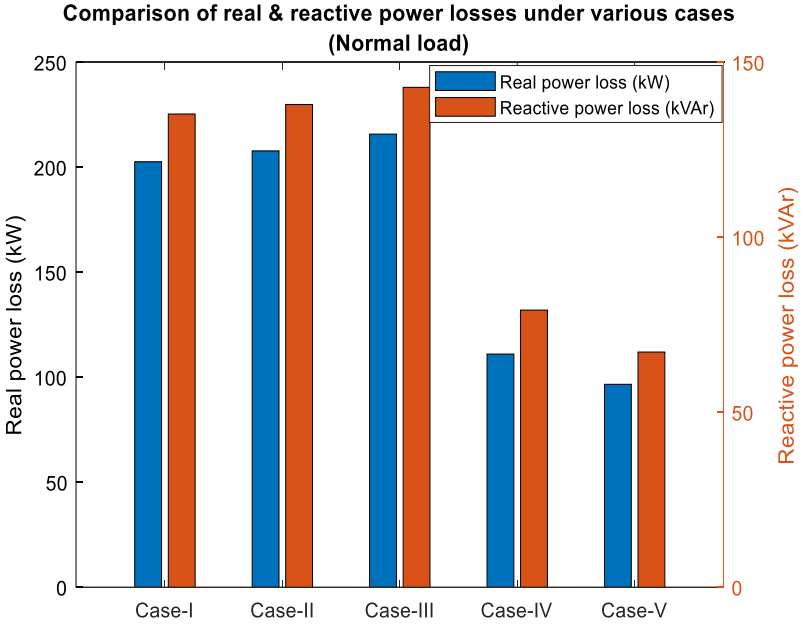

Figure 8. Effect of EVCSs on real and reactive power losses on normal load (1.0).

Illustrated in Figure 9 is a graphical depiction of how EVCSs influence real and reactive power losses, specifically when the system operates at peak load conditions (1.6), involving a load equivalent to 160% of the normal power load. The adopted approach yields noteworthy results by substantially curbing power losses. This observation underscores

the prowess of the SHOA in effectively addressing the power loss predicament arising from the integration of EVCS. This efficacy is particularly pronounced when the system operates under regular load conditions.

Demonstrated in Figure 10 is a visual representation of the real power loss profile, showcasing the outcomes of implementing the proposed SHOA across various distinct cases. Notably, among all the cases under consideration, it becomes evident that Case V, which incorporates two HFC-DGs, stands out as the superior performer in terms of loss reduction across all levels of the bus network. Comparative analysis underscores the distinct advantage of Case V in consistently achieving enhanced loss reduction across the entire bus network. This finding underscores the efficacy of integrating two HFC-DGs in Case V and how it positively influences the system's overall efficiency. The remarkable performance of Case V relative to the other cases solidifies the value proposition of leveraging SHOA in conjunction with the strategic integration of HFC-DGs to effectively optimize power loss reduction across the distribution network.

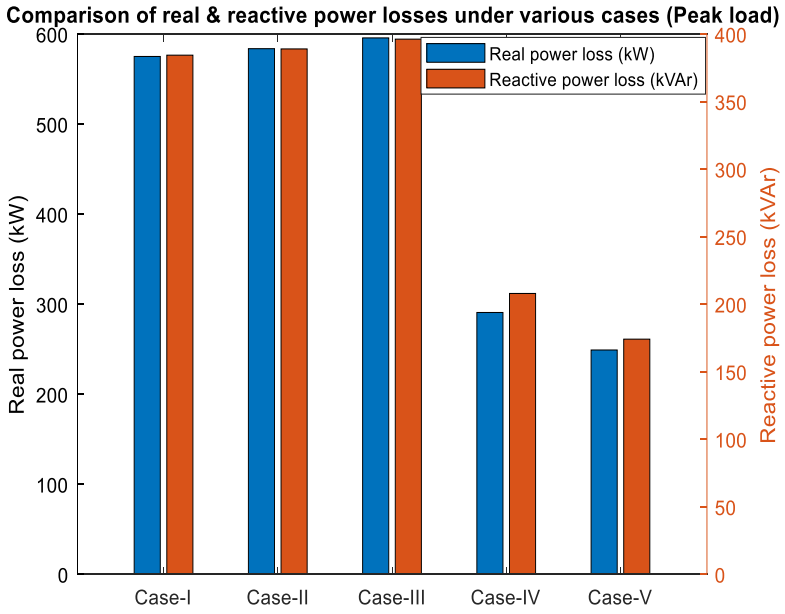

Figure 9. Effect of EVCSs on real and reactive power losses on peak load (1.6).

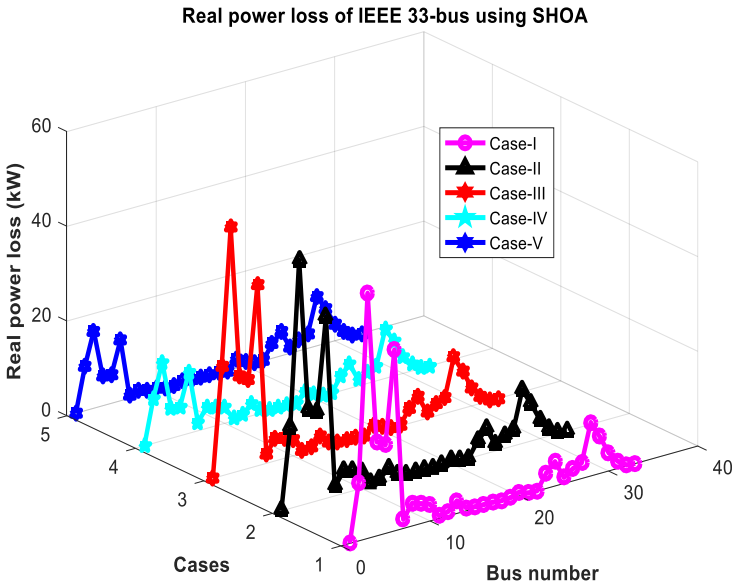

Figure 10. Real power loss profile employing the proposed SHOA under various cases.

5.2.2. The Influence of EVCSs on the Voltage Characteristics of the System

Incorporating EVCSs into the RDS negatively impacts both the voltage profile and voltage stability index (VSI). The introduction of EVs adds further strain to the system, leading to a decrease in the voltage profile and voltage stability. To mitigate these disturbances, HFC-DG units are strategically installed at specific locations within the RDS. A visual representation of the voltage profile evolution in a 33-bus system is depicted in Figure 11, illustrating the implementation of EVCSs and HFC-DGs using the SHOA. As the charging demand grows, there is a gradual decline in the voltage at each bus, as illustrated in Figure 11. However, when two EVCSs with a power rating of 1932 kW are strategically placed at buses 2 and 19, the overall voltage profile of the system decreases. Moreover, as the quantity of EVCSs increases, the voltage profile also rises.

The integration of HFC-DG units and EVCSs in the RDS promotes efficient operation and positively affects the voltage profile. The analysis presented in Figure 11 reveals voltage fluctuations across all buses due to actual and reactive power losses in the distribution system. To counteract these losses and enhance voltage levels, support in the form of real power is necessary. Such assistance helps mitigate losses caused by resistance (I^2R losses). Research indicates that an optimal configuration of two HFC-DG units within the RDS leads to improved bus voltages. The specific type, size, and placement of HFC-DGs significantly influence the enhancement of the voltage profile. As shown in Table 1, the installation of two HFC-DGs in the 33-bus system results in a rise in the minimum voltage from 0.9118 p.u. to 0.9521 p.u. A thorough examination of the data confirms that the SHOA provides a more substantial enhancement of the voltage profile, as depicted in Figure 11.

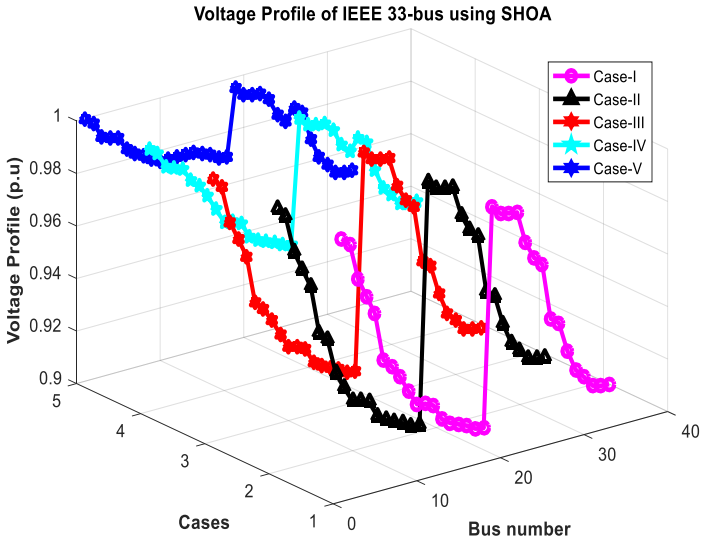

Figure 11. Voltage profile employing the proposed SHOA under various cases.

5.2.3. Effect of EVCSs on System Reliability

In this study, reliability indices are utilized to analyze the impact of merging EVCS and HFC-DG units on the overall reliability of the system. These indices are calculated based on quantifiable data such as failure and repair rates, average outage duration, and the number of customers at each load point. The study investigates various dependability indices including SAIFI, SAIDI, CAIDI, EENS, AENS, ASAI, and ASUI to thoroughly examine how the placement of EVCS and HFC-DG units affects the reliability of the IEEE 33-bus system. After integrating EVCSs and HFC-DG, the reliability indices are evaluated for different cases. The numerical values of failure rate, repair rate, and average outage duration which were collected from the references [36,37] were coded using SHOA in MATLAB environment to calculate the reliability indices component values of (i) Average failure rate, (ii) Annual outage duration, and (iii) Average outage duration. With the help of these values, the main reliability indices (SAIFI, SAIDI, CAIDI, EENS, AENS, ASAI,

and ASUI) of the distribution system were calculated. The introduction of EVCSs led to a decrease in both customer-oriented and load-based dependability indices. However, incorporating HFC-DGs into the system resulted in an improvement in both types of dependability indices. This improvement can be attributed to the effective management of bus voltage by HFC-DGs, which enhances power transfer capacity and reduces power loss by regulating the supplied power to the system. By controlling the injected power, HFC-DGs directly impact the power flow. The statistics presented in Table 3 indicate a decline in reliability indices after the installation of EVCS. In the baseline scenario, the SAIFI value was recorded as 0.0982 failures per customer per year. However, after installing an EVCS on bus 2, the SAIFI value increased to 0.1197 failures per customer per year. Similarly, with one EVCS assigned to bus 2, the SAIDI and CAIDI values rose to 0.5238 h/customer/yr and 4.9114 h/customer/interruption, respectively.

Table 3. Various reliability indicators in the 33-bus RDS.

Cases	SAIFI	SAIDI	CAIDI	EENS	AENS	ASAI	ASUI
Case I	0.0982	0.5048	5.1405	1780	1.9369	0.9999	0.0001
Case II	0.1287	0.6321	4.9114	9390.12	9.9854	0.9998	0.0002
Case III	0.1401	0.7155	5.1071	14,905.24	15.8758	0.9995	0.0005
Case IV	0.1197	0.5238	4.3759	8684.88	9.1547	0.9996	0.0004
Case V	0.1097	0.4714	4.2971	6494.35	6.9094	0.9997	0.0003

Integrating a single EVCS into the RDS has a negative impact on both the EENS and AENS indices. Initially, the AENS baseline value is recorded at 1.9369 MWh/customer/yr, but after incorporating the EVCS, it rises to 9.1547 MWh/customer/yr. This increase in AENS indicates a greater shortfall in meeting the load demands, which is undesirable for the distribution system. Moreover, the ASAI, which represents electricity availability, decreases as the charging loads increase due to the introduction of the EVCS. When evaluating the reliability indices with two EVCSs located at buses 2 and 19 in the RDS, it is observed that distributing the EVCSs across multiple nodes leads to higher reliability compared to concentrating them at a single node.

In scenarios where powerful nodes in the power grid coincide with densely trafficked nodes in the transportation network, a significant finding has emerged. This finding highlights the issue of congestion in the pathways leading to these specific nodes, especially when charging electric vehicles. By distributing EVCSs, the charging capability becomes accessible to a broader range of EVs traveling on different routes. As a result, this distribution helps alleviate traffic congestion on the specific paths that lead to the concentrated charging loads on buses. Introducing a certain amount of energy can also enhance the reliability of the RDS. One effective approach is to utilize HFC-DGs, which have the ability to inject active and reactive power into the system as needed. Incorporating two HFC-DGs into the network results in significant enhancements in system reliability. Table 3 provides a concise overview of the impact of integrating HFC-DGs on dependability measures. Upon connecting a single HFC-DG to bus 6, the SAIFI value experiences a decline to 0.1197 failures per user annually. Likewise, the SAIDI and CAIDI values decrease to 0.5238 h/customer/yr and 4.3759 h/customer/interruption, respectively. The reliability indices continue to decrease further with the addition of more HFC-DGs to the network. Consequently, this decrease in disturbance duration and number of interruptions leads to lower SAIDI and SAIFI values, ultimately enhancing the reliability of the RDS.

It is significant to acknowledge that as the number of HFC-DGs combined into the RDS increases, the EENS and AENS values show a decline. To illustrate, when only one HFC-DG is present, the AENS value amounts to 9.1547 MWh/customer/yr. However, with the addition of another HFC-DG, this value decreases to 6.9094 MWh/customer/yr. The inclusion of multiple HFC-DGs in the network improves the energy supply and reduces the metrics associated with energy not supplied. This reduction in EENS and AENS values is highly desirable as it contributes to a more dependable power system. Consequently, the incorporation of DGs with reliable data has a positive impact on reliability indices

related to electrical supply, such as ASAI and ASUI. With the integration of more HFC-DGs, the ASAI values increase, resulting in a decrease in ASUI, ultimately enhancing the overall reliability of the system. The graphs in Figure 12a–g illustrate the influence of EVCSs and HFC-DG units on reliability indicators in the 33-bus RDS. Among all scenarios, Case V, featuring two HFC-DGs, consistently outperforms others in enhancing reliability indices. This highlights the significant benefits of employing multiple HFC-DGs, suggesting improved load distribution, resilience, and response to contingencies.

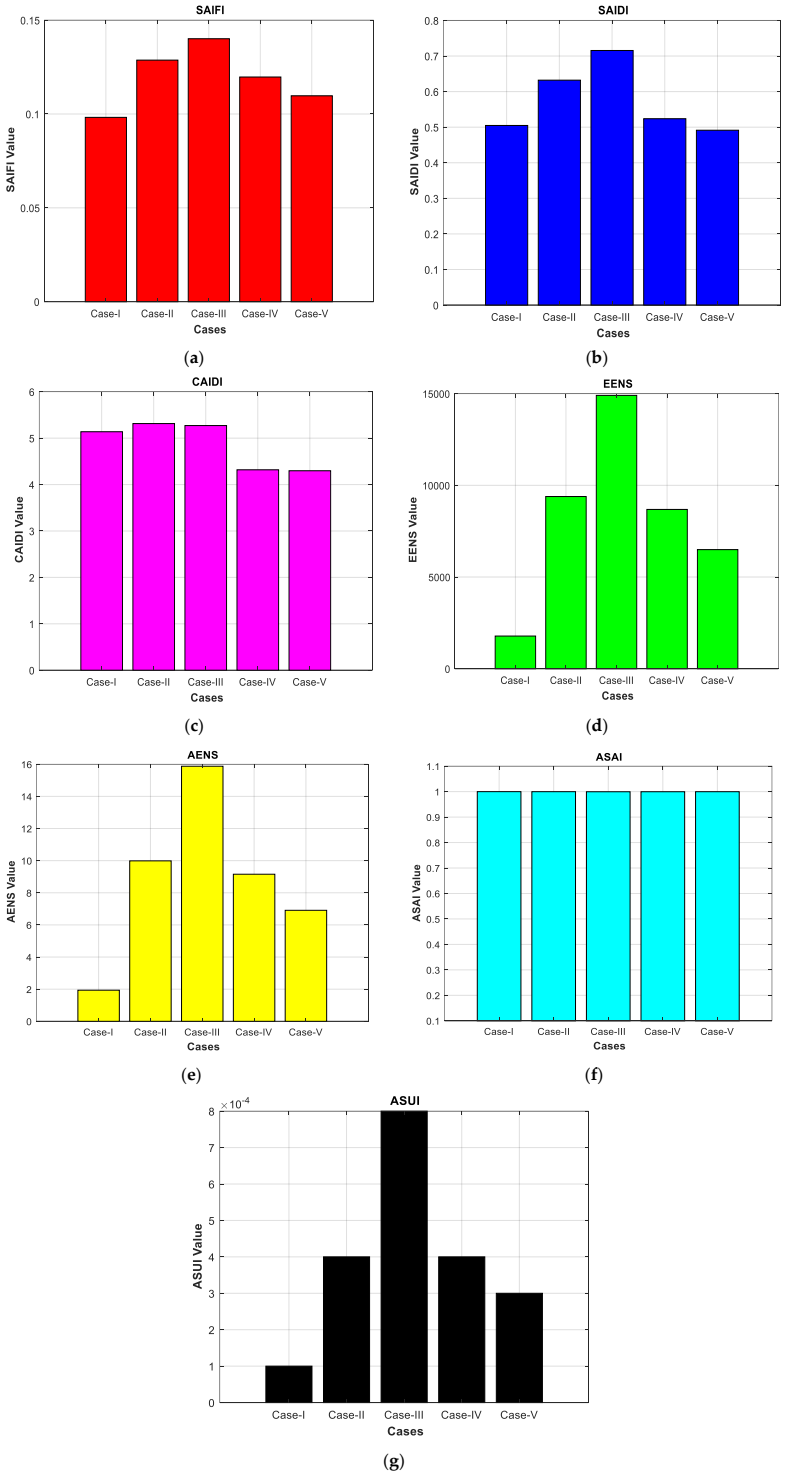

Figure 12. Variation in reliability indices with EVCS and HFC-DG inclusion: (**a**) SAIFI, (**b**) SAIDI, (**c**) CAIDI, (**d**) EENS, (**e**) AENS, (**f**) ASAI, and (**g**) ASUI.

5.3. Overall Comparative Analysis

The efficacy of the SHOA was assessed in the context of minimizing power losses within the standardized IEEE 33-test system. Uniform base values were adopted for cases I, II, and III across all algorithms, ensuring a fair basis for comparison. Common locations, sizes, power loss magnitudes, and other relevant parameters were maintained across all strategies. A comprehensive comparison involving the BA, AVOA, and BESA was conducted against SHOA's performance.

The optimized values derived from each approach were consolidated into Table 4, unveiling a consistent pattern that positioned the SHOA method as a frontrunner in power loss reduction across all examined cases. Figure 13 visually shows the comparison of real power loss values among the various algorithms under distinct cases. Specifically, in Case V, SHOA outperformed alternative algorithms (BA—103.46 kW, AVOA—127.53 kW, and BESA—121.99 kW), demonstrating more effective loss reduction (Table 4 and Figure 13).

Table 4. Comparative analysis of results under various optimization algorithms.

Cases	Parameter	SHOA	BA	AVOA	BESA
Case I (Without Compensation)	P_{loss} (kW)	202.67	202.67	202.67	202.67
	Q_{loss} (kVAr)	135.24	135.24	135.24	135.24
	V_{min} (p.u.)	0.9131	0.9131	0.9131	0.9131
	VSI_{min} (p.u.)	0.6890	0.6890	0.6890	0.6890
Case II (With One EVCS)	Optimum size (kW) and position of EVCS	966 (2)	966 (2)	966 (2)	966 (2)
	P_{loss} (kW)	207.84	207.84	207.84	207.84
	Q_{loss} (kVAr)	137.95	137.95	137.95	137.95
	V_{min} (p.u.)	0.9124	0.9124	0.9124	0.9124
	VSI_{min} (p.u.)	0.6871	0.6871	0.6871	0.6871
	Convergence time (s)	10.39	11.25	14.02	12.59
Case III (With Two EVCSs)	Optimum size (kW) and position of EVCS	966 (2) 966 (19)	966 (2) 966 (19)	966 (2) 966 (19)	966 (2) 966 (19)
	P_{loss} (kW)	215.82	215.82	215.82	215.82
	Q_{loss} (kVAr)	142.86	142.86	142.86	142.86
	V_{min} (p.u.)	0.9118	0.9118	0.9118	0.9118
	VSI_{min} (p.u.)	0.6853	0.6853	0.6853	0.6853
	Convergence time (s)	11.47	13.17	14.82	13.95
Case IV (With Two EVCSs and One HFC-DG)	Optimum size (kW) and position of EVCS	966 (2) 966 (19)	966 (2) 966 (19)	966 (2) 966 (19)	966 (2) 966 (19)
	Optimum size (kW) and position of HFC-DG	2500 (6)	2080 (8)	1500 (11)	950 (16)
	P_{loss} (kW)	111.08	117.62	145.79	130.36
	% P_{loss} Reduction	48.53	45.5	32.45	39.6
	Q_{loss} (kVAr)	79.21	81.15	97.66	87.24
	V_{min} (p.u.)	0.9487	0.9459	0.9308	0.9373
	VSI_{min} (p.u.)	0.8041	0.7924	0.7424	0.7636
	Convergence time (s)	13.06	14.98	15.48	14.58
Case V (With Two EVCSs and Two HFC-DGs)	Optimum size (kW) and position of EVCS	966 (2) 966 (19)	966 (2) 966 (19)	966 (2) 966 (19)	966 (2) 966 (19)
	Optimum size (kW) and position of HFC-DG	1900 (6) 600 (14)	1150 (8) 1400 (27)	1500 (11) 300 (22)	950 (16) 1080 (25)
	P_{loss} (kW)	96.67	103.46	127.53	121.99
	% P_{loss} Reduction	55.21	52.06	40.91	43.48
	Q_{loss} (kVAr)	67.23	71.80	85.38	83.79
	V_{min} (p.u.)	0.9521	0.9513	0.9379	0.9341
	VSI_{min} (p.u.)	0.8136	0.8102	0.7656	0.7531
	Convergence time (s)	14.22	16.42	17.03	16.02

This outcome underscores SHOA's role as a superior strategy for heightening power system performance. Furthermore, the proposed optimization methodology, centered around SHOA, showcased superior efficacy in enhancing voltage profiles compared to competing methods (SHOA—0.9521 p.u., BA—0.9513 p.u., AVOA—0.9379 p.u., and BESA—0.9341 p.u.). Additionally, SHOA consistently yielded superior minimum VSI values (SHOA—0.8136 p.u., BA—0.8102 p.u., AVOA—0.7656 p.u., and BESA—0.7531 p.u.) in the context of Case V. These findings underscore SHOA's capacity to adeptly address intricate power system challenges.

Table 4 presents a comprehensive performance evaluation of the IEEE 33-bus system using various algorithms across different cases. Among these, Case V serves as the primary focus for comparison, representing the crux of the analysis involving HFC-DG and EVCS allocation within the RDS. Notably, the performance contrasts between Case V and other cases are highlighted in this table. Specifically, for the purpose of illustration and analysis,

Figures 14 and 15 provide a visual depiction of power loss profiles and voltage profiles in the context of Case IV. The comparison is centered on the IEEE 33-bus RDS and pertains to the proposed algorithm and existing optimization methods. Notably, these visualizations are limited to Case V, given its pivotal role in the assessment. From the insights garnered in Figures 14 and 15, it becomes evident that the proposed SHOA yields superior outcomes in terms of loss reduction and voltage profile enhancements, outperforming alternative optimization algorithms within the IEEE 33-bus RDS. Particularly, the SHOA approach showcases the most notable loss reduction of 96.67 kW, though this value is relatively lower compared to other methodologies. Additionally, the SHOA stands out with its minimum bus voltage of 0.9521 p.u., which surpasses the results attained by other algorithms.

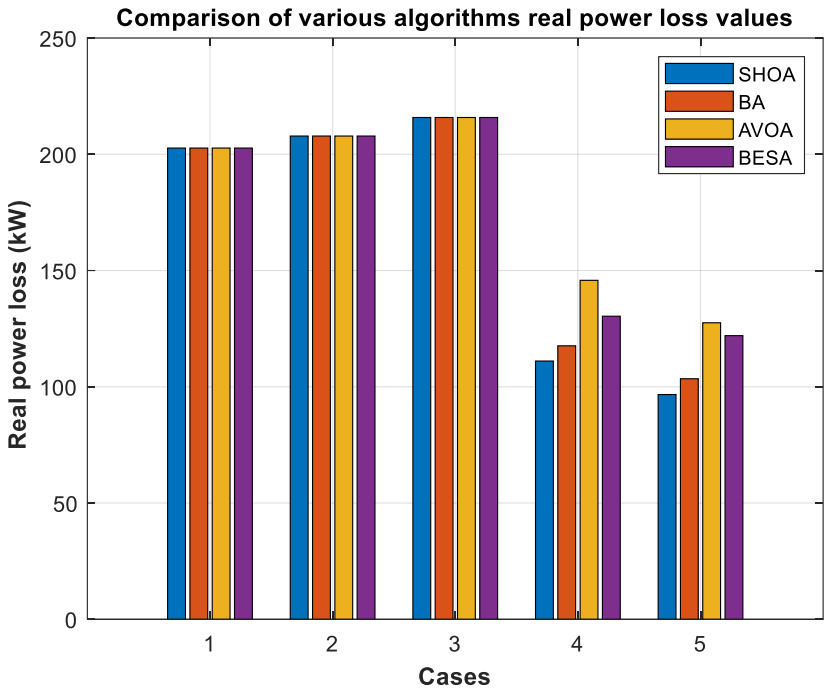

Figure 13. Comparison of various algorithms real power loss values under various cases.

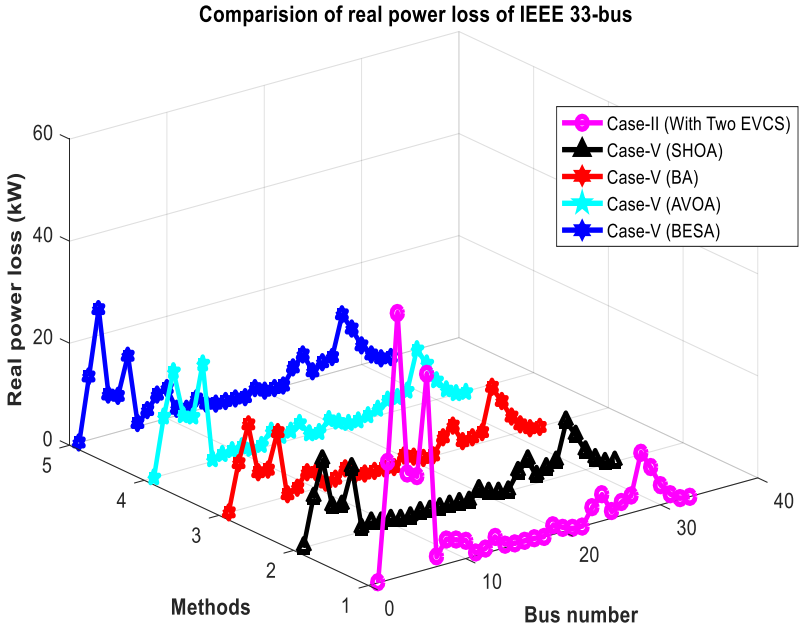

Figure 14. Comparison of real power loss profile using various algorithms (Case V).

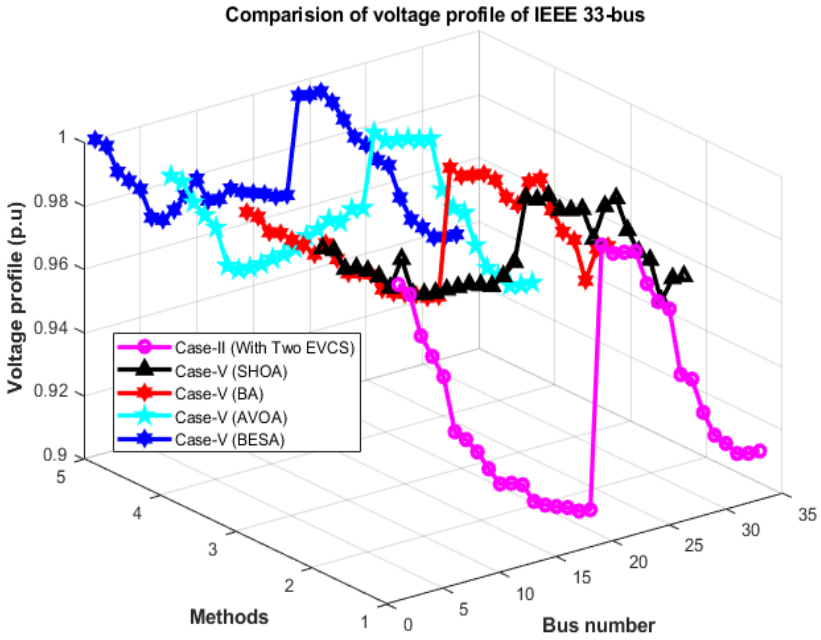

Figure 15. Comparison of voltage profile using various algorithms (Case V).

Based on the above discussions, the integration of HFC-DG coupled with the strategic application of the recommended SHOA proves instrumental in mitigating the adverse consequences posed by EVCSs on the RDS. This collaborative approach not only effectively curtails the negative influence of EVCSs but also significantly enhances the overall reliability of the power system.

The effectiveness of an algorithm's ability to reach solutions approaching the global optimum hinges on the consistency of its convergence. In Figure 16, a comparison of convergence patterns is presented for the 33-bus test system among various well-known algorithms, including BA, AVOA, and BESA. This serves as a precursor to understanding the performance of the SHOA algorithm. Impressively, the SHOA algorithm achieves convergence to the optimal objective value within a mere nine iterations, outshining its counterparts in terms of convergence speed. What sets SHOA apart is its remarkable convergence rate, characterized by both stability and swiftness, along with a remarkable capacity for near-global exploration to identify optimal HFC-DG sizes. The algorithm consistently maintains a swift convergence pace overall, notably excelling in comparison to the other tested algorithms in both its speed and accuracy of convergence.

Table 5 provides a comprehensive performance comparison of the main case (Case V) using different algorithms (SHOA, BA, AVOA, and BESA), focusing on key factors such as real power loss, minimum bus voltage, VSI, and convergence time. This assessment includes a contrast with alternative algorithms. Remarkably, the SHOA consistently outperforms competitors by minimizing both real and reactive power losses across all cases. SHOA's dominance as a strategy for enhancing RDS performance becomes evident. It significantly improves voltage profiles in contrast to other techniques. Notably, VSI_{min} values consistently show improvement under SHOA across all cases, indicating its effectiveness in stabilizing the system. A standout feature is SHOA's rapid convergence, achieving optimal solutions in just nine iterations with 14.22 s for Case V. This highlights its computational efficiency and problem-solving prowess.

Further, the performance of various optimization algorithms was rigorously evaluated under diverse reliability indicators for the main Case V, as demonstrated in Table 6. Strikingly, the results unequivocally underscore the exceptional reliability enhancement achieved through the implementation of the proposed SHOA. When juxtaposed with its counterparts—BA, AVOA, and BESA—SHOA consistently emerges as the superior choice. The remarkably lower values across critical reliability indices such as SAIFI, SAIDI, CAIDI,

EENS, AENS, ASAI, and ASUI clearly establish SHOA's effectiveness in fortifying the distribution system against interruptions and outages. This compelling evidence firmly positions SHOA as a robust and promising tool for bolstering the reliability and resilience of the entire system and its operation in Renewable Hydrogen Energy Communities [38]. The combined utilization of HFC-DG units and SHOA effectively mitigates the impact of EVCSs on the RDS, underscoring its potential to enhance distribution network sustainability and efficiency and enlarging the set of performances monitored in an interpretable way [39].

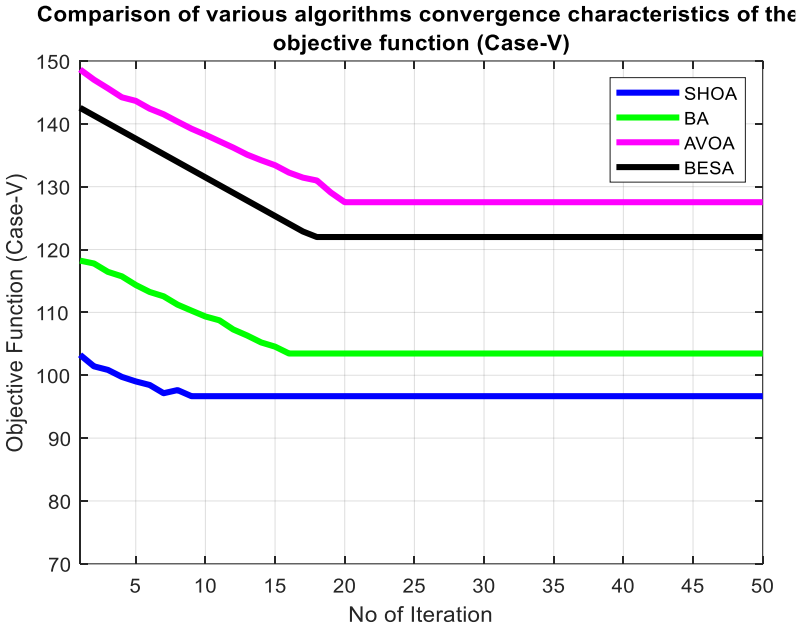

Figure 16. Comparison of various algorithms convergence characteristics of the objective function (Case V).

Table 5. Performance of system under different algorithms with key factors (Case V).

Methods	P_{loss} (kW)	Q_{loss} (kVAr)	V_{min} (p.u.)	VSI_{min} (p.u.)	Convergence Time (s)
SHOA	96.67	67.23	0.9521	0.8136	14.22
BA	103.46	71.8	0.9513	0.8102	16.42
AVOA	127.53	85.38	0.9379	0.7656	17.03
BESA	121.99	83.79	0.9341	0.7531	16.02

Table 6. Performance of system under different algorithms with various reliability indicators (Case V).

Methods	SAIFI	SAIDI	CAIDI	EENS	AENS	ASAI	ASUI
SHOA	0.1097	0.4714	4.2971	6494.35	6.9094	0.9997	0.0003
BA	0.1099	0.4926	4.4822	6499.98	6.9096	0.9997	0.0003
AVOA	0.1114	0.4938	4.4326	6512.19	6.9099	0.9995	0.0005
BESA	0.1103	0.4933	4.4723	6502.13	6.9098	0.9996	0.0004

6. Conclusions

Electric vehicles offer a viable solution to reduce transportation pollution, leading to an increased demand for EVCSs. However, the rapid growth of EVCSs can negatively impact the distribution network, necessitating the evaluation of suitable locations for these stations. Additionally, by incorporating reliability considerations into the allocation strategy, the RDS can confirm an uninterruptible power supply, voltage stability, customer satisfaction, and resilience in the face of operational changes and disruptions. Moreover, the utilization of HFC-DG shows significant promise in generating clean and sustainable power within the distribution system, enhancing efficiency, resilience, and environmental sustainability. The current study focused on a novel approach to enhance the placement

of HFC-DG with EVCSs to reduce power loss and improve the reliability of the RDS. A unique SHOA inspired by nature is proposed and implemented to identify and size the HFC-DG and EVCS. The aim is to mitigate the impact of EVCSs on the RDS by strategically allocating suitable HFC-DG using the SHOA-based optimization technique. The efficiency and feasibility of the suggested methods are evaluated using the standard IEEE 33-bus test system. The simulation results demonstrate that the primary objective of the study has been successfully achieved with the support of the SHOA. The proposed technique leads to significant reductions in power loss and improvements in reliability across different load levels. The allocation of multiple HFC-DGs with EVCSs proves beneficial in terms of power loss mitigation, reliability enhancement, and improvements in bus voltage and VSI in the distribution system. Overall, the integration of HFC-DGs provides a reliable and sustainable solution for minimizing the impact of EVCS on the RDS. The main innovations of the presented study are described as:

- The research introduced HFC-DG integration in an RDS for EVCS impact reduction with a novel approach.
- Varied load levels (Light, Normal, Peak) and battery capacities (20 kWh, 10 kWh, 16 kWh) were considered.
- SHOA was employed for EVCS and HFC-DG allocation, showcasing its optimization potential.
- Reliability analysis was prioritized, enhancing system dependability and resilience.
- A comparative study evaluated SHOA, BA, AVOA, and BESA on an IEEE 33-bus RDS.

The research demonstrated the superiority of the proposed approach through rigorous performance analysis.

Author Contributions: All authors have contributed equally to the idea and the design of the methodology proposed and to the deployment of the research paper. Conceptualization, T.Y.; methodology, T.Y. and T.D.S.; software, T.Y. and A.A.C.; validation, T.D.S., A.A.C. and T.S.B.; formal analysis, T.Y. and T.S.B.; investigation, T.Y. and B.N.; resources, B.N.; writing—original draft preparation, T.Y. and A.A.C.; writing—review and editing, T.S.B.; visualization, T.S.B.; supervision, T.S.B. and B.N.; project administration, B.N. All authors have read and agreed to the published version of the manuscript.

Funding: This research received no external funding.

Data Availability Statement: Not applicable.

Conflicts of Interest: The authors declare no conflict of interest.

References

1. Ahmad, F.; Iqbal, A.; Ashraf, I.; Marzband, M. Optimal location of electric vehicle charging station and its impact on distribution network: A review. *Energy Rep.* **2022**, *8*, 2314–2333. [CrossRef]
2. Yuvaraj, T.; Devabalaji, K.R.; Thanikanti, S.B.; Aljafari, B.; Nwulu, N. Minimizing the electric vehicle charging stations impact in the distribution networks by simultaneous allocation of DG and DSTATCOM with considering uncertainty in load. *Energy Rep.* **2023**, *10*, 1796–1817.
3. Jung, J.W.; Keyhani, A. Fuel cell based distributed generation system. In Proceedings of the 2008 12th International Middle-East Power System Conference, Aswan, Egypt, 12–15 March 2008; IEEE: New York, NY, USA, 2008; pp. 610–616.
4. Fathi, S.H.; Rastegar, H.; Ghadimi, A.A. Control of islanded industrial networks with fuel cell based distributed generation units and ultra-capacitor storage device. *Eur. Trans. Electr. Power* **2011**, *21*, 801–823. [CrossRef]
5. Das, S.; Das, D.; Patra, A. Operation of solid oxide fuel cell based distributed generation. *Energy Procedia* **2014**, *54*, 439–447. [CrossRef]
6. Hariri, A.M.; Hejazi, M.A.; Hashemi-Dezaki, H. Reliability optimization of smart grid based on optimal allocation of protective devices, distributed energy resources, and electric vehicle/plug-in hybrid electric vehicle charging stations. *J. Power Sources* **2019**, *436*, 226824. [CrossRef]
7. Jannati, J.; Nazarpour, D. Optimal energy management of the smart parking lot under demand response program in the presence of the electrolyser and fuel cell as hydrogen storage system. *Energy Convers. Manag.* **2017**, *138*, 659–669. [CrossRef]
8. Dharavat, N.; Sudabattula, S.K.; Velamuri, S.; Mishra, S.; Sharma, N.K.; Bajaj, M.; Elgamli, E.; Shouran, M.; Kamel, S. Optimal allocation of renewable distributed generators and electric vehicles in a distribution system using the political optimization algorithm. *Energies* **2022**, *15*, 6698. [CrossRef]
9. Hadian, E.; Akbari, H.; Farzinfar, M.; Saeed, S. Optimal allocation of electric vehicle charging stations with adopted smart charging/discharging schedule. *IEEE Access* **2020**, *8*, 196908–196919. [CrossRef]

10. Shojaabadi, S.; Abapour, S.; Abapour, M.; Nahavandi, A. Simultaneous planning of plug-in hybrid electric vehicle charging stations and wind power generation in distribution networks considering uncertainties. *Renew. Energy* **2016**, *99*, 237–252. [CrossRef]
11. Srinivas, D.; Reddy, M.R. Optimal Placement of Electric Vehicle Charging Station by Considering Dynamic Loads in Radial Distribution System. In Proceedings of the 2022 International Conference on Automation, Computing and Renewable Systems (ICACRS), Pattaya, Thailand, 19–21 March 2022; IEEE: New York, NY, USA, 2022; pp. 212–217.
12. Liu, Z.; Wen, F.; Ledwich, G. Optimal planning of electric-vehicle charging stations in distribution systems. *IEEE Trans. Power Deliv.* **2012**, *28*, 102–110. [CrossRef]
13. Bhadoriya, J.S.; Gupta, A.R.; Zellagui, M.; Saxena, N.K.; Arya, A.K.; Bohre, A.K. Optimal allocation of electric vehicles charging station in distribution network beside DG using TSO. In *Planning of Hybrid Renewable Energy Systems, Electric Vehicles and Microgrid: Modeling, Control and Optimization*; Springer Nature Singapore: Singapore, 2022.
14. Gampa, S.R.; Jasthi, K.; Goli, P.; Das, D.; Bansal, R.C. Grasshopper optimization algorithm based two stage fuzzy multiobjective approach for optimum sizing and placement of distributed generations, shunt capacitors and electric vehicle charging stations. *J. Energy Storage* **2020**, *27*, 101117. [CrossRef]
15. De Lima, T.D.; Franco, J.F.; Lezama, F.; Soares, J.; Vale, Z. Joint optimal allocation of electric vehicle charging stations and renewable energy sources including CO_2 emissions. *Energy Inform.* **2021**, *4*, 33. [CrossRef]
16. Hemmatpour, M.H.; Koochi, M.H.R.; Dehghanian, P.; Dehghanian, P. Voltage and energy control in distribution systems in the presence of flexible loads considering coordinated charging of electric vehicles. *Energy* **2022**, *239*, 121880. [CrossRef]
17. Mohanty, A.K.; Suresh Babu, P.; Salkuti, S.R. Optimal Allocation of Fast Charging Station for Integrated Electric-Transportation System Using Multi-Objective Approach. *Sustainability* **2022**, *14*, 14731. [CrossRef]
18. Adetunji, K.E.; Hofsajer, I.W.; Abu-Mahfouz, A.M.; Cheng, L. A novel dynamic planning mechanism for allocating electric vehicle charging stations considering distributed generation and electronic units. *Energy Rep.* **2022**, *8*, 14658–14672. [CrossRef]
19. Salkuti, S.R. Binary Bat Algorithm for Optimal Operation of Radial Distribution Networks. *Int. J. Electr. Eng. Inform.* **2022**, *14*, 148–160. [CrossRef]
20. Ahmadi, M.; Rastgoo, S.; Mahdavi, Z.; Nasab, M.A.; Zand, M.; Sanjeevikumar, P.; Khan, B. Optimal allocation of EVs parking lots and DG in micro grid using two-stage GA-PSO. *J. Eng.* **2023**, *2023*, e12237. [CrossRef]
21. Krishnamurthy, N.K.; Sabhahit, J.N.; Jadoun, V.K.; Gaonkar, D.N.; Shrivastava, A.; Rao, V.S.; Kudva, G. Optimal Placement and Sizing of Electric Vehicle Charging Infrastructure in a Grid-Tied DC Microgrid Using Modified TLBO Method. *Energies* **2023**, *16*, 1781. [CrossRef]
22. Balu, K.; Mukherjee, V. Optimal allocation of electric vehicle charging stations and renewable distributed generation with battery energy storage in radial distribution system considering time sequence characteristics of generation and load demand. *J. Energy Storage* **2023**, *59*, 106533. [CrossRef]
23. Yuvaraj, T.; Devabalaji, K.R.; Thanikanti, S.B.; Pamshetti, V.B.; Nwulu, N. Integration of Electric Vehicle Charging Stations and DSTATCOM in Practical Indian Distribution Systems using Bald Eagle Search Algorithm. *IEEE Access* **2023**, *11*, 55149–55168. [CrossRef]
24. Sriabisha, R.; Yuvaraj, T. Optimum placement of Electric Vehicle Charging Station using Particle Swarm Optimization Algorithm. In Proceedings of the 2023 9th International Conference on Electrical Energy Systems (ICEES), Chennai, India, 23–25 March 2023; IEEE: New York, NY, USA, 2023; pp. 283–288.
25. Pompern, N.; Premrudeepreechacharn, S.; Siritaratiwat, A.; Khunkitti, S. Optimal Placement and Capacity of Battery Energy Storage System in Distribution Networks Integrated with PV and EVs Using Metaheuristic Algorithms. *IEEE Access* **2023**, *11*, 68379–68394. [CrossRef]
26. Yang, X.S.; He, X. Bat algorithm: Literature review and applications. *Int. J. Bio-Inspired Comput.* **2013**, *5*, 141–149. [CrossRef]
27. Abdollahzadeh, B.; Gharehchopogh, F.S.; Mirjalili, S. African vultures optimization algorithm: A new nature-inspired metaheuristic algorithm for global optimization problems. *Comput. Ind. Eng.* **2021**, *158*, 107408. [CrossRef]
28. Alsattar, H.A.; Zaidan, A.A.; Zaidan, B.B. Novel meta-heuristic bald eagle search optimisation algorithm. *Artif. Intell. Rev.* **2020**, *53*, 2237–2264. [CrossRef]
29. Dhiman, G.; Kumar, V. Spotted hyena optimizer: A novel bio-inspired based metaheuristic technique for engineering applications. *Adv. Eng. Softw.* **2017**, *114*, 48–70. [CrossRef]
30. Teng, J.H. A direct approach for distribution system load flow solutions. *IEEE Trans. Power Deliv.* **2003**, *18*, 882–887. [CrossRef]
31. Huang, X.; Zhang, Z.; Jiang, J. Fuel cell technology for distributed generation: An overview. In Proceedings of the 2006 IEEE International Symposium on Industrial Electronics, Montreal, QC, Canada, 9–13 July 2006; IEEE: New York, NY, USA, 2006; Volume 2, pp. 1613–1618.
32. Hosseini, S.J.A.D.; Moradian, M.; Shahinzadeh, H.; Ahmadi, S. Optimal placement of distributed generators with regard to reliability assessment using virus colony search algorithm. *Int. J. Renew. Energy Res.* **2018**, *8*, 714–723.
33. Singh, M.; Kumar, P.; Kar, I. Implementation of vehicle to grid infrastructure using fuzzy logic controller. *IEEE Trans. Smart Grid* **2012**, *3*, 565–577. [CrossRef]
34. Kumar, S.; Sarita, K.; Vardhan, A.S.S.; Elavarasan, R.M.; Saket, R.K.; Das, N. Reliability assessment of wind-solar PV integrated distribution system using electrical loss minimization technique. *Energies* **2020**, *13*, 5631. [CrossRef]
35. Sahoo, N.C.; Prasad, K. A fuzzy genetic approach for network reconfiguration to enhance voltage stability in radial distribution systems. *Energy Convers Manag.* **2006**, *47*, 3288–3306. [CrossRef]

36. Deb, S.; Tammi, K.; Kalita, K.; Mahanta, P. Impact of electric vehicle charging station load on distribution network. *Energies* **2018**, *11*, 178. [CrossRef]
37. Bilal, M.; Rizwan, M.; Alsaidan, I.; Almasoudi, F.M. AI-based approach for optimal placement of EVCS and DG with reliability analysis. *IEEE Access* **2021**, *9*, 154204–154224. [CrossRef]
38. Nastasi, B.; Mazzoni, S. Renewable Hydrogen Energy Communities layouts towards off-grid operation. *Energy Convers. Manag.* **2023**, *291*, 117293. [CrossRef]
39. Manfren, M.; James, P.A.B.; Aragon, V.; Tronchin, L. Lean and interpretable digital twins for building energy monitoring—A case study with Smart Thermostatic Radiator Valves and Gas Absorption Heat Pumps. *Energy AI* **2023**, 100304. [CrossRef]